gels

MDPI

Review

Drug-Releasing Conductive Hydrogels for Brain–Computer Interface Electrodes: Materials, Biosafety, and Regulatory Considerations

Jiajia Zang [1], Yaya Cui [1], Yucheng Gao [1], Qiong Yan [1], Yue Wang [2], Chunqing Zhang [2,*] and Haibin Wang [1,*]

[1] College of Life Sciences and Bioengineering, School of Physical Science and Engineering, Beijing Jiaotong University, Beijing 100044, China
[2] National Institutes for Food and Drug Control, Beijing 102629, China
* Correspondence: zhangchunq@nifdc.org.cn (C.Z.); wanghb@bjtu.edu.cn (H.W.)

Abstract

The long-term stability of brain–computer interface (BCI) electrodes depends not only on the quality of neural signal acquisition but also on mechanical mismatch at the electrode–neural tissue interface, chronic inflammation, glial scarring, and progressive signal attenuation. Conductive hydrogels combine high water content, low modulus, and favorable interfacial conformity, allowing them to mitigate several limitations of conventional neural electrodes and making them promising materials for BCI electrode design. However, improvements in flexibility and conductivity alone are insufficient to address implantation-induced foreign-body responses. Drug-releasing conductive hydrogels additionally incorporate anti-inflammatory agents, neurotrophic factors, or immunomodulatory molecules into conductive hydrogel networks. While maintaining electrical signal transmission and interfacial conformity, these systems may also modulate local inflammation, glial activation, and neuronal retraction. Existing reviews have largely focused on the functional material design of hydrogel-based BCI interfaces, with limited attention to the regulatory considerations associated with their clinical translation. This review examines the matrix materials, conductive components, and interfacial functionalization strategies of conductive hydrogels, with particular emphasis on drug-delivery approaches and their potential applications in BCI neural electrodes. From a drug–device combination product perspective, we further discuss product classification and biological safety evaluation requirements within the regulatory frameworks of China, the United States, and the European Union, with the aim of informing material development, clinical translation, and science-based regulation.

Keywords: brain–computer interface; electrode materials; conductive hydrogel; drug delivery; drug-device combination product; science-based regulation

Check for updates

Academic Editor: Louisa Windus

Received: 29 September 2026
Revised: 10 November 2026
Accepted: 12 November 2026
Published: 15 November 2026

Copyright: © 2026 by the authors. Licensee MDPI, Basel, Switzerland. This article is an open access article distributed under the terms and conditions of the Creative Commons Attribution (CC BY) license.

1. Introduction

A brain–computer interface (BCI) enables direct communication between the brain and external devices by acquiring, decoding, and modulating neural activity. In recent years, implantable BCIs have achieved major advances in cursor control, robotic arm grasping, handwriting decoding, and speech neuroprostheses for individuals with paralysis, demonstrating substantial potential for clinical translation [1–4]. These studies show that neural activity in the motor cortex and language-related regions can be recorded over extended periods and translated into executable control signals. However, the long-term stability, reproducibility, and scalability of clinical BCI systems depend not only on advances in

decoding algorithms and electronic hardware but also critically on the stability of the neural electrode-brain tissue interface.

BCIs are generally classified as noninvasive, semi-invasive, or invasive according to the extent of tissue penetration and the site of signal acquisition. Noninvasive systems record, from the scalp, electrical potentials generated by populations of cortical neurons after attenuation through the skull and scalp. Although relatively safe, these signals are prone to attenuation and have limited spatial resolution. Semi-invasive systems are placed on the cortical surface and therefore record population-level cortical activity more directly, with higher signal-to-noise ratios and spatial resolution than noninvasive systems, but they require stable conformity to the brain surface. Invasive systems record local field potentials and neuronal action potentials, providing higher signal resolution. However, electrode implantation can disrupt the blood–brain barrier and permit the extravasation of blood-derived proteins. These events subsequently activate microglia and astrocytes and promote inflammation and glial scar formation. These overlapping and evolving processes ultimately lead to neuronal loss, increased electrode impedance, and reduced signal quality [5–7] (Figure 1).

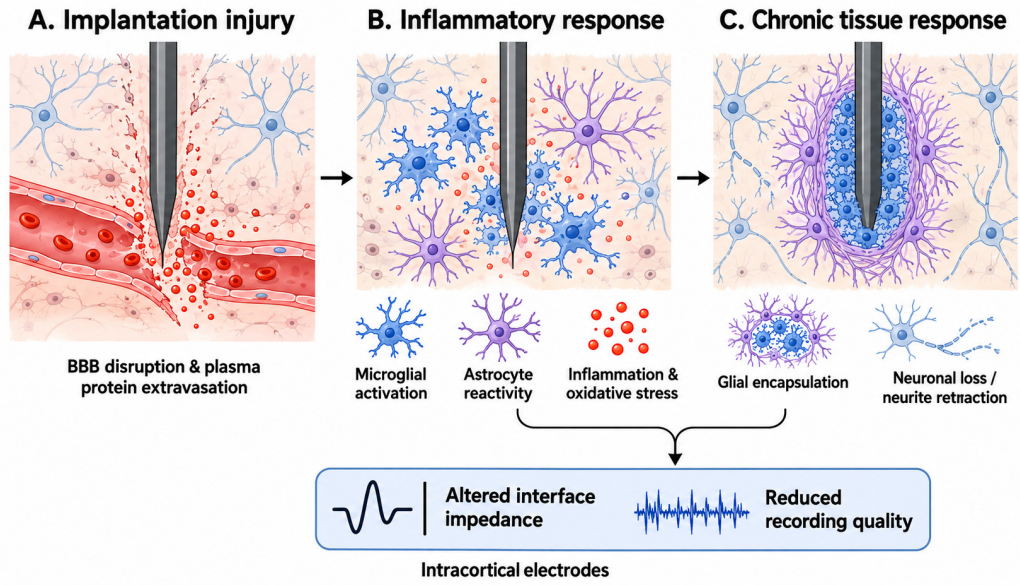


Figure 1. Dynamic progression of the foreign-body response and signal degradation following neural electrode implantation.

Conventional neural electrodes are commonly fabricated from platinum, iridium, gold, silicon, carbon-based materials, or flexible polymers such as polyimide and polydimethylsiloxane (PDMS). Metals and silicon offer excellent conductivity and microfabrication compatibility, but their stiffness is substantially greater than that of brain tissue, making chronic implants susceptible to local injury caused by mechanical mismatch and tissue micromotion [8]. Flexible polymers reduce stiffness but are intrinsically weak conductors and therefore generally require integration with metals or conductive coatings [9]. For chronically implanted electrodes, material-tissue contact is not a simple physical interface but a continuously evolving biological interface. Implantation-induced blood–brain barrier disruption, local inflammation, and activation of microglia and astrocytes progressively promote glial scar formation, increase electrode impedance, and degrade signal quality [10–12] (Figure 1).

Conductive hydrogels offer a materials-based strategy for addressing these limitations. Hydrogels are highly hydrated materials consisting of hydrophilic polymer networks, and their mechanical properties and aqueous microenvironment more closely resemble those of soft tissues. Conductive hydrogels that combine softness with electrical conductivity can be created by incorporating conductive polymers, carbon-based nanomaterials, MXenes, metal nanomaterials, liquid metals, or ionic conductors [13–15]. These materials can reduce mechanical mismatch at the electrode-tissue interface and facilitate ionic and electronic transport, thereby improving neural recording and electrical stimulation. Kim et al. noted that conductive and functional hydrogels and their nanocomposites can serve as key interfacial materials for soft implantable bioelectronics. Their application to neural signal recording may improve both mechanical and electrical coupling between electronic devices and soft tissues [16].

Nevertheless, enhancing conductivity and flexibility alone is insufficient for chronic BCI electrodes. Failure of invasive electrodes arises from long-term interactions among the implanted material, electrode, neural tissue, and immune response. Accordingly, greater flexibility and conductivity cannot fully prevent chronic inflammation and glial scarring after implantation. Recent efforts have therefore focused on engineering conductive hydrogels as interfacial materials that combine electrical conduction with local biological regulation. Conductive hydrogels can improve electrode–tissue conformity and electrical coupling. Related drug-releasing coatings, layered electrode architectures, and neural-repair hydrogels provide evidence for local anti-inflammatory delivery, neurotrophic support, and immunomodulation. These functions have been demonstrated at different levels of integration and in different anatomical settings; they should not be interpreted as capabilities already established together in a single chronic conductive-hydrogel BCI electrode [12,17–20]. Shen et al. systematically reviewed the composition, conductive mechanisms, and biomedical applications of conductive hydrogels and noted that these materials can further integrate drug delivery, mechanotransduction, and immunomodulation, providing a materials platform for multifunctional neural interfaces [21].

This review examines how incorporating local drug delivery into conductive hydrogel interfaces for BCI electrodes changes material selection, electrode performance, and the evidence needed to evaluate the finished device (Table 1). Hydrogel composition and network structure govern how a therapeutic agent is retained and released. Drug loading and release can, in turn, alter hydrogel swelling and interfacial charge transfer, with consequences for neural recording or stimulation. A key unresolved question is whether the same electrode can achieve effective drug exposure at the target site while maintaining electrical function during release and after reservoir depletion. By tracing these relationships, we identify which findings from material and release studies can inform electrode design and which questions require testing of the finished device. This distinction guides our comparison of regulatory considerations in China, the United States, and the European Union.

Table 1. Comparison of the present review with selected reviews on conductive hydrogels for neural interfaces, implantable bioelectronics, and drug delivery.

Review (Year)	Main Focus	Drug Delivery	Neural Electrode Performance	Chronic Biological Response	Drug–Device Regulatory Analysis	Distinct Contribution of the Present Review	Ref.
Sagdic et al. (2023)	Hydrogels for implantable bioelectronics	Limited	Covered	Covered	—	—	[22]
Dawit et al. (2024)	Conductive hydrogels for neural recording and stimulation	Limited	Main focus	Covered	—	—	[23]
Cheng et al. (2024)	Hydrogel coatings, electrodes, and neural interfaces	Covered	Main focus	Covered	—	—	[14]
Xue et al. (2025)	Fabrication, properties, and neural applications	Covered	Main focus	Covered	—	—	[24]
Ghosh et al. (2025)	Electrically responsive hydrogels for on-demand delivery	Main focus	Limited	Limited	—	—	[25]
Present review	Drug-releasing conductive hydrogels for BCI electrodes	Main focus	Covered	Covered	Dedicated discussion	Integrates release strategies, electrode function, chronic tissue responses, and drug–device regulation; distinguishes direct electrode evidence from related delivery systems.	—

2. Review Methodology

This review draws on representative studies to critically discuss material design and therapeutic delivery at neural electrode interfaces, rather than cataloguing all conductive hydrogel formulations. We focused on original research published between 2021 and 2026, while retaining earlier work that established key mechanisms or reported relevant neural electrode experiments. Studies were selected for their relevance to the target interface, the detail of material and device characterization, the availability of quantitative results and testing conditions, and their value in explaining design trade-offs. Neither journal impact factor nor positive findings determined inclusion or the weight given to a study. Review articles were used for background and to identify original studies, rather than as experimental evidence.

We considered what each system integrated, where it was tested, and how far it had been validated. For therapeutic functionalization, we classified a study as direct integrated evidence only when a conductive hydrogel formed part of an electrode and both therapeutic release and electrical function were experimentally demonstrated in the same system. Conductive hydrogel electrodes without drug delivery, drug-releasing nonconductive coatings, conducting-polymer films, and therapeutic nanostructures were discussed as supporting approaches for future integration. Findings from cardiac interfaces, peripheral nerves, tissue-repair scaffolds, and general delivery systems were identified by their original application and were not taken as evidence of efficacy in brain electrodes. We also distinguished bench and cell experiments from acute animal studies, chronic preclinical studies, and clinical evaluations. Demonstrating integration therefore did not, by itself, establish long-term performance or clinical readiness.

The discussion covers different hydrogel matrices, conductive components, therapeutic functions, and release mechanisms, with separate consideration of scalp, cortical-surface, and intracortical interfaces. For each representative study, we examined the reported benefits alongside limitations such as instability, swelling, delamination, burst release, payload depletion, and limited biological validation. Where reported, we considered the controls, experimental model, sample size, variability, testing conditions, and observation period. Electrical and mechanical results were interpreted in the context of electrode geometry and measurement methods. Drug-release duration was recorded separately from implantation or follow-up duration, and missing parameters were left unreported rather than estimated. This was a qualitative appraisal, without a formal risk-of-bias tool or numerical quality score. The representative selection and differences among studies limit direct comparisons: selection and publication bias remain possible, and the evidence does not support estimates of how common particular findings are or an overall ranking of material systems.

3. Material Design and Integration of Conductive Hydrogel Neural Electrodes

Conductive hydrogels can improve the contact between electronic devices and biological tissue, but their design requirements depend on where that contact is established. A scalp electrode must maintain coupling through the stratum corneum and accommodate hair, sweat, and movement, whereas a cortical-surface array operates in a persistently wet environment and must follow tissue deformation without compromising spatial selectivity. A penetrating electrode additionally faces insertion constraints and tissue displacement within the brain. These requirements cannot be reduced to a single conductivity or modulus target. This section therefore considers the shared material principles before comparing application-specific evidence and the integration strategies needed to preserve function over time. Studies involving peripheral nerves, spinal cord, cardiac tissue, or in vitro neural

models are identified as supporting evidence rather than treated as direct demonstrations of a brain interface.

The performance of conductive hydrogel electrodes emerges from the combined effects of matrix chemistry, conducting-phase organization, and device architecture. These choices create coupled trade-offs among charge transport, mechanical compliance, swelling, and interfacial stability, which must be balanced against the distinct requirements of scalp, cortical-surface, and intracortical interfaces (Figure 2).

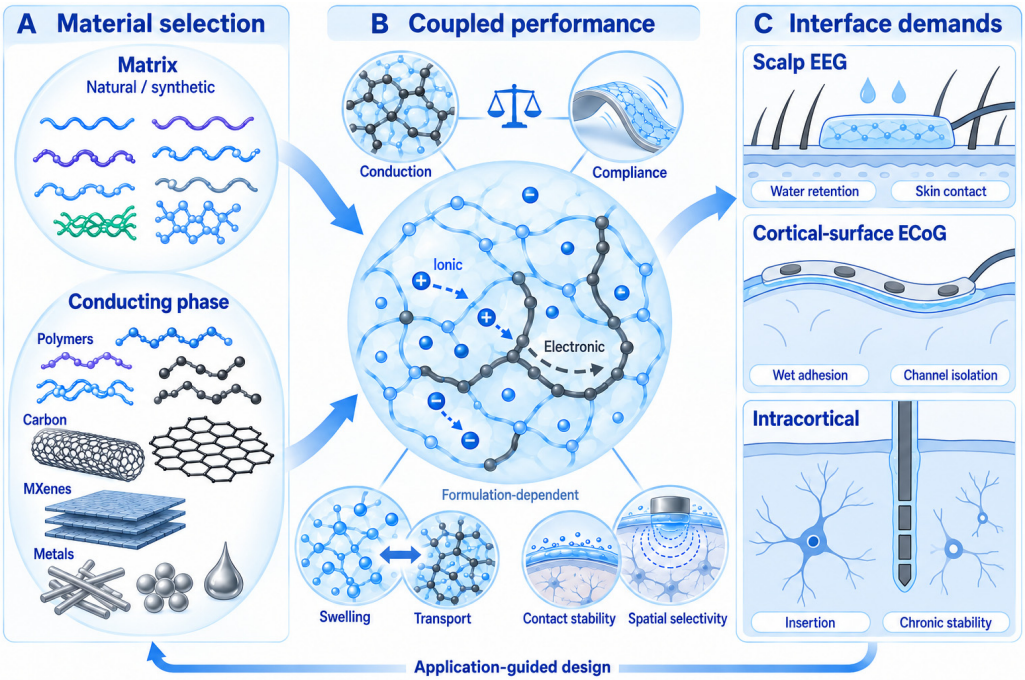


Figure 2. Interrelationships among material selection, coupled performance, and application requirements for conductive hydrogel neural interfaces.

3.1. Hydrogel Matrices and Conductive Networks

The hydrogel matrix provides the hydrated environment in which charge transport and mechanical deformation occur. Its suitability for a neural interface depends on crosslink density, polymer interactions, solvent composition, and network architecture, rather than simply on whether the polymer is natural or synthetic. Natural polymers can form strong networks, while synthetic polymers can be formulated to achieve tissue-like compliance. For example, an all-natural cellulose–bentonite hydrogel combined an ionic conductivity of 89.9 mS/cm at 25 °C with a compressive strength of up to 3.2 MPa [26]. This combination illustrates the range of properties accessible with natural matrices, although high strength and freezing tolerance are not sufficient criteria for brain implantation. The more relevant question is how the hydrated network behaves at the dimensions and loading conditions of the intended electrode.

At a neural electrode, the matrix must also accommodate a conducting phase without obstructing charge transfer or contact with neural tissue. One approach is to form the conducting network within an existing biological polymer scaffold. A conducting network of poly(3,4-ethylenedioxythiophene) (PEDOT) doped with polystyrene sulfonate (PSS) was formed within gelatin methacrylate (GelMA), producing patternable microelectrode coatings with reversible electroactivity and lower impedance than bare gold or GelMA-coated microelectrodes [27]. A related integration strategy used a PEDOT hydrogel electrode mesh with poly(styrene-ethylene-butylene-styrene) (SEBS) substrates and encapsulation

to establish an electrical interface with human neural organoids [28]. In both cases, the hydrated matrix supports the conducting structure while the device architecture defines the recording interface. These results establish useful fabrication and neural-interfacing approaches, although microelectrode and organoid experiments do not reproduce the insertion injury, cerebrospinal-fluid exposure, and immune response encountered in an intact brain.

Maintaining a continuous electronic pathway becomes more difficult as water content increases and the polymer matrix separates conducting domains. Raising the conductive filler content can improve connectivity, but may reduce compliance or produce a less uniform network. Organizing the conducting phase offers an alternative to simply adding more of it. A poly(acrylic acid) (PAA) template was used to guide PEDOT assembly, yielding a hydrogel with a conductivity of 247 S/cm, approximately 90 wt% water, a modulus of 25 kPa, and stretchability of 610% [29]. By comparison, assembling polypyrrole (PPy) around an aramid-nanofiber/poly(vinyl alcohol) (PVA) network produced a conductivity of approximately 80 S/cm, strength of approximately 9.4 MPa, and stretchability of approximately 36% [30]. Together, these systems illustrate how template selection changes the balance between electrical connectivity, strength, and deformation. The former was demonstrated in sciatic-nerve stimulation and cardiac recording, and the latter in cardiomyocyte experiments; their relevance to brain electrodes therefore lies primarily in the network-design principles they establish.

A continuous conducting phase must nevertheless be supported by a network that resists fracture and permits device fabrication. Bicontinuous architectures address this requirement by assigning electrical and mechanical functions to interconnected networks. Conducting-polymer and hydrophilic-polyurethane networks, for example, combined conductivity above 11 S/cm with stretchability above 400% and fracture toughness above 3300 J/m^2 in physiological environments, while also supporting multimaterial 3D printing [31]. The hydrophilic network provides mechanical integrity without fully interrupting conduction, allowing the formulation to be developed into a monolithic structure. For an implanted device, the remaining challenge is to retain these pathways and the adhesion between printed regions during repeated deformation and prolonged hydration; fracture toughness alone does not establish fatigue resistance.

Fabrication methods determine whether such network properties can be preserved at electrode-relevant dimensions. Liquid-in-liquid printing of PEDOT hydrogels enabled tunable three-dimensional structures with conductivities up to 301 S/m, illustrating how mechanics and conduction can be controlled spatially [32]. At smaller dimensions, laser-induced phase separation produced PEDOT hydrogel patterns with 6 µm resolution, conductivity up to 670 S/cm, and electrochemical stability over six months in a physiological environment [33]. These approaches extend material design into control over electrode shape and feature size. Their reported endpoints should, however, remain distinct: six-month material stability is not equivalent to six-month in vivo recording, and a fabricated feature size does not by itself determine neural recording resolution.

Conducting phases can also be arranged at interfaces or within separate layers, rather than distributed uniformly throughout the hydrogel. This is particularly useful when the conductor and hydrated matrix have markedly different deformation behavior. A graphene–hydrogel interface redirected cracking and dissipated deformation, improving intrinsic stretchability by more than fivefold [34]. A laminated PVA/liquid-metal hydrogel achieved a maximum conductivity of 217,895 S/m together with high tensile strength and extensibility [35]. In the latter system, conduction depended on liquid-metal self-sintering at the bottom surface. These examples show that conductor placement can be as important as composition, but also explain why conductivity

values from different architectures are not directly interchangeable. Transport direction, conductor distribution, and exposed conducting area must be specified before a surface-dominated pathway is compared with bulk conduction through a uniformly hydrated network.

Beyond network geometry, the nature of charge transport determines how a hydrogel functions within an electrode. Mobile ions carry charge through the aqueous phase, whereas connected electronic conductors carry charge along the electrode and its interconnects. At the electrolyte-facing surface, these processes are coupled through interfacial electrochemistry. Consequently, bulk conductivity alone cannot establish the relative ionic and electronic contributions or predict stimulation performance. Conductivity comparisons should be accompanied by frequency-dependent impedance, electrode geometry, hydration state, and measurement configuration. A moderately conductive material may provide adequate coupling over a short distance, while a highly conductive material may still fail because of poor adhesion or insufficient interconnect insulation [27,29,31,33].

The electrochemical processes that enable charge transfer can also alter the conducting network. Reduction in PEDOT decreases the population of electronic charge carriers and requires ionic compensation within the hydrated polymer. The resulting redistribution of ions and water may change its volume. Reversible volumetric charging can increase accessible charge storage, but excessive polarization may impair conduction and promote irreversible damage. In electrodeposited PEDOT on gold, a cathodic stability limit of approximately −0.6 V versus Ag|AgCl was identified, with stable charge injection of 3.6 mC/cm^2 at a 200 µs pulse width over 200 million pulses [36]. These film measurements provide a mechanistic reference for hydrogel design, rather than a universal operating limit. The usable stimulation range of each hydrated formulation must be established under its intended waveform through voltage-transient measurements and assessment of electrochemical drift and irreversible changes.

The distinction between material conductivity and device function becomes particularly important when hydrogels are used in active electronics. An n-type semiconducting hydrogel enabled complementary circuits and electrophysiological signal amplification [37], while polymer semiconductors incorporated into double-network hydrogels achieved tissue-level moduli as low as approximately 81 kPa and charge-carrier mobilities up to 1.4 cm^2/(V·s) [38]. These developments expand the role of hydrogels from passive contacts to signal-processing components. Their performance cannot, however, be assessed using electrode conductivity alone: mobility, transistor gain, interface impedance, and stimulation capacity describe different functions. Translation into chronic neural devices will require evaluation of the complete circuit, including leakage, operating bias, and the stability of the aqueous semiconductor interface.

Matrix and conducting-network selection should therefore begin with the intended electrical and mechanical function. Conductivity needs to be interpreted alongside water content and transport direction, while strength, modulus, and fracture toughness describe separate aspects of mechanical behavior. Likewise, cell compatibility does not establish chronic device performance [26–35,37,38]. The central design objective is to preserve the required properties after physiological equilibration, patterning, and integration, so that a promising bulk material becomes a reliable electrical contact at a defined neural interface.

3.2. Application-Specific Requirements and Material Design

For scalp electroencephalography (EEG), material design is governed primarily by the need to maintain conductive contact across the stratum corneum despite hair, evaporation, and movement. Semidry electrodes address this problem by storing electrolyte in a compliant structure and supplying it locally during use. An eight-channel noninvasive brain–computer interface (BCI) incorporating silver nanowires, PVA hydrogel, and melamine sponge maintained system impedance of approximately 8–14 kΩ during a three-hour motion-onset visual evoked potential task [39]. Separate ten-hour tracking at P7/P8 showed impedance of approximately 6–8.5 kΩ. These results link electrolyte retention and structural compliance to a functioning scalp interface, while also illustrating the need to distinguish contact stability from decoding performance: the ten-hour impedance measurements did not establish ten-hour task performance.

Maintaining hydration is only part of the problem, because the electrode must also remain attached during sweating and movement. Self-adhesive PVA/poly(vinylpyrrolidone) (PVP) hydrogels containing polydopamine nanoparticles supported wireless prefrontal EEG under these conditions, with a seven-category sustained-attention classification accuracy of 91.5% [40]. Separating conduction and substrate adhesion into two hydrogel layers provided another route to stable contact, supporting N170/P300 acquisition and twelve-hour wear [41]. In that study, reuse over fourteen days consisted of two-hour daily sessions. Together, these approaches show how adhesion and hydration can be addressed through composition or layered architecture. Their application outcomes nevertheless depend on wearing location, task, and acquisition conditions; classification accuracy is not an intrinsic material property, and repeated daily use is different from uninterrupted monitoring.

The same dependence on test conditions applies to impedance. In the bilayer system, sub-kilohm bench measurements differed substantially from human scalp measurements, where real-time impedance remained below 150 kΩ over twelve hours [41]. Electrode pressure, contact area, skin condition, measurement frequency, and acquisition electronics all contribute to the measured value. A low impedance obtained with a fixture or skin model therefore cannot establish superior human EEG performance. For scalp applications, the more informative endpoint is stable, low-noise acquisition under the intended wearing and task conditions.

Progressive dehydration remains a limitation even when initial contact is satisfactory. Combining ionic conduction with graphite-mediated electronic transport in a hyaluronic-acid gel partially compensated for this loss, with the optimized formulation retaining conductivity of 1.84 S/m after seventy-two hours [42]. Human evaluation involved twenty-four-hour wear, EEG sampling at defined time points, and twenty-four working electrodes with initial contact impedance adjusted below 10 kΩ. The material and human tests address related but different questions: retention of conductivity for seventy-two hours does not establish EEG performance over the same period or show that every channel remained below its initial impedance. Further assessment under repeated use, hair, and prolonged skin exposure is needed to determine how effectively this strategy sustains practical scalp contact.

At the cortical surface, the design priorities shift from preventing evaporation to maintaining wet adhesion, dimensional stability, and electrical isolation between channels. An ultrasoft adhesive hydrogel containing dopamine-modified PEDOT nanoparticles was developed to improve contact with brain tissue and limit adverse tissue responses [43]. This approach brings adhesion into the conducting-phase design, but stronger attachment must be balanced against swelling and the forces required for removal. Effective cortical coatings

need to stabilize the interface without imposing excessive tissue loading or compromising the spatial selectivity of the array.

These requirements extend beyond the tissue-facing coating to the full multilayer device. A sixteen-channel, four-layer all-hydrogel array incorporated a PEDOT conducting layer between encapsulation layers and an MXene-containing shielding layer [44]. The system achieved a reported maximum conductivity of 4176 S/cm, approximately 15-μm patterning, and a signal-to-noise ratio (SNR) roughly tenfold higher than that of a commercial silver electrode, with cortical-surface recording and tissue assessment including two-week results. A complementary approach used a zwitterionic poly(sulfobetaine methacrylate) (pSB) matrix with PEDOT and NaCl to prioritize compliance and resistance to fouling [45]. This formulation had a conductivity of approximately 9 S/m and a Young's modulus of 1.74 kPa; integration with gold electrocorticography (ECoG) electrodes supported rat cortical recording at implantation and at two weeks, as shown in the supporting Information of Ref. [45]. These examples illustrate different routes to a functional cortical interface: multilayer integration can combine conduction, encapsulation, and shielding, while a compliant antifouling coating can improve contact without maximizing bulk conductivity. In either case, pattern dimensions, material stability, and in vivo function require separate interpretation. The 15 μm pattern width does not establish equivalent neural resolution, and the four-week PBS mass-retention assay of the zwitterionic material does not extend its demonstrated recording duration.

Longer-term cortical recording further highlights the importance of device geometry and hydration state. A 128-channel conducting-polymer hydrogel array with an interfacial percolation microstructure (CHIP) was 9 μm thick and exhibited an in vivo interface impedance of 8.9 ± 1.2 kΩ at 1 kHz, with the longest postimplantation recording extending to 550 days [46]. Its in-plane conductivity decreased from 2512 ± 118 S/cm at 36.4% water content to 235 ± 47 S/cm at 85.9% water content. Moreover, the complete array had an effective modulus of 61.3 MPa despite containing soft hydrogel components. Conformability therefore arose from the thin geometry and layered construction as well as the constituent materials. The study provides extended recording evidence, but the longest recording interval, sixteen-week histology, and PBS stability tests remain distinct endpoints; they should not be combined into a claim of uninterrupted recording or equivalent-duration biological assessment. For cortical arrays more broadly, hydrated channel isolation must also be demonstrated, since an all-hydrogel construction does not itself guarantee effective sealing.

Penetrating electrodes introduce an additional conflict: the device must resist buckling during insertion yet remain mechanically accommodating after implantation. A soft coating can improve the tissue-facing interface, but it does not remove the stiffness or displacement associated with the underlying shank. Covalent anchorage and crosslinking strengthened the conducting-hydrogel/metal interface and supported neural recording in freely moving mice and electrical modulation [47]. This strategy addresses coating attachment, a prerequisite for preserving the benefits of a hydrated interface. Its value must be assessed together with coating thickness and shank geometry, because additional coating volume or delamination can offset improvements in material compliance.

Layered coatings offer another way to assign conducting and tissue-interfacing functions to different components. PEDOT and poly(2-hydroxyethyl methacrylate) (pHEMA) coatings on a flexible probe with a cross-section of 300 μm × 2.5 μm supported recording and stimulation in the rat hippocampus, including induction of long-term potentiation [48]. Here, PEDOT provides the conducting surface, and pHEMA modifies the hydrated interface, rather than forming a homogeneous mixed conducting hydrogel. Ionic hydrogels provide a further alternative. A microgel-crosslinked formulation, HM-2, had a modulus of 59.7 kPa

and high extensibility; when placed in a polyimide-coated silica capillary with a 450-µm outer diameter, it enabled local field potential (LFP) recording from hippocampal cornu ammonis area 1 (CA1) in freely moving rats over four weeks [49]. A separate microelectrode configuration supported single-neuron recording with a spike SNR of 7.2 dB. These studies demonstrate different ways to construct a penetrating neural interface, but their device-level interpretation is essential: long-term potentiation is a physiological outcome rather than an implant-lifetime measure, and the modulus of HM-2 does not describe the mechanics of its capillary-supported device. The LFP and spike configurations must also remain distinct when relating electrode dimensions to performance.

The properties of a penetrating coating may also change after implantation as it equilibrates with body temperature and the surrounding fluid. A PNIPAM-derived fibrous network combined with conducting polythiophene altered hydration and recovery behavior, with body temperature improving the electrical response [50]. Recordings from the mouse somatosensory thalamus were examined through six weeks, alongside histology at one, three, and six weeks. Spiking nevertheless declined by week six in both coated and bare probes, indicating that improved interfacing did not eliminate chronic signal deterioration. This result underscores the need to follow electrical performance over time rather than infer durability from favorable initial material properties. As with the hippocampal studies, the thalamic application should remain anatomically distinct from intracortical validation.

Adding drug delivery creates further demands on the geometry and stability of a penetrating interface. Independently addressable conductive-hydrogel microneedles provided a direct example of cortical penetration with both neural recording and electrically controlled drug release [51]. Neural recording exceeded three hours, while implant-associated tissue responses were assessed over four weeks. The architecture demonstrates that conducting networks, recording sites, and drug reservoirs can be integrated within a penetrating device. However, the four-week tissue assessment does not establish four weeks of continuous closed-loop treatment. The therapeutic control and dosing implications of this system are discussed in Section 4.

These application differences provide a practical basis for matrix selection. For scalp electrodes, electrolyte retention, controlled evaporation, and attachment at hair-bearing sites are generally more relevant than biodegradation, as illustrated by the PVA-based semidry electrode and the hyaluronic-acid formulation [39,42]. At the cortical surface, dimensional stability and resistance to protein adsorption favor controlled networks, including zwitterionic formulations; penetrating coatings additionally require secure anchorage and restricted expansion [45,47,52]. Biological polymers supply functional groups for cell interactions and drug binding, whereas synthetic networks allow systematic adjustment of crosslinking and integration between layers. Neither origin alone determines suitability. For drug-releasing implants, reservoir capacity must also be balanced against swelling and recording-site dimensions. This differs from scalp EEG, where an electrolyte reservoir primarily maintains skin coupling rather than treating inflammation at an implanted interface [27,39,51].

The intended clinical task also determines how long these properties must be retained. Clinical recording periods range from short diagnostic sessions to many years of assistive use. A comparison in 100 patients evaluated 30 min routine EEG against 24 h ambulatory recording [53], while a separate intracranial epilepsy-monitoring cohort had median monitoring periods of seven days for subdural electrodes and eight days for stereotactic or hybrid configurations [54]. At a much longer timescale, an implanted ECoG BCI supported home communication for seven years in one person with amyotrophic lateral sclerosis, and intracortical microstimulation was evaluated across implant durations of two to ten years in five participants [55,56]. These conventional devices illustrate clinical timescales rather

than demonstrated hydrogel lifetimes. A resorbable architecture may be appropriate for temporary use only if function persists throughout the monitoring period and degradation products can be safely cleared. Chronic applications instead require contact and insulation to remain stable over the intended service life. Biodegradability should therefore be evaluated against the required treatment or recording interval, rather than presented as an inherent advantage.

Across all three interfaces, comparison is most useful when the reported endpoint matches the intended application. Scalp studies need to distinguish continuous wear, repeated use, intermittent signal sampling, and decoding sessions. Cortical-surface arrays require information on channel geometry, crosstalk, functional spatial resolution, and changes in in vivo impedance. Penetrating devices additionally require insertion dimensions, the actual brain region, recording yield, and tissue responses at relevant depths. Impedance from a complete scalp acquisition system cannot be ranked directly against a three-electrode PBS measurement or an implanted microelectrode, just as a low material modulus or high SNR cannot establish superior chronic performance without the corresponding device dimensions and recording conditions [39,41,42,44,46,48–51]. Future comparisons will be more informative when material characterization is linked to these device-level and application-specific outcomes.

3.3. Interfacial Stability and Device Integration

The initial performance of a conductive hydrogel electrode can be sustained only if tissue contact, conducting pathways, and insulated interconnects remain stable during use. The dominant failure mechanisms differ across applications. Scalp electrodes must retain hydration and adhesion despite evaporation and repeated handling, whereas implanted devices face swelling, mechanical fatigue, biofouling, and insulation failure. A conductive-polymer/hydrogel scalp electrode maintained favorable electrode–skin impedance over a twenty-nine-day comparison period, illustrating the potential for extended contact performance [57]. Practical service life nevertheless depends on how the electrode is stored, reused, and worn; a comparison period of this length does not imply uninterrupted EEG recording.

For implanted hydrogels, dimensional stability is a prerequisite for maintaining contact without increasing tissue loading. Swelling measured in an unrestricted aqueous environment may not reflect behavior within the brain, where geometry and local fluid availability constrain water uptake. Studies of initially dehydrated, ultrasoft hydrogel shanks showed that re-swelling depended on implant geometry and water availability at the hydrogel–tissue interface [52]. This makes dehydration-assisted insertion a coupled material–tissue process rather than a temporary change in material stiffness alone. Dimensional recovery and the resulting local loading must therefore be considered together.

Controlling swelling during fabrication offers a way to address this problem throughout the device. Anti-swelling hydrogel building blocks developed for embedded printing included a biphasic conducting ink that, after aqueous equilibration, reached conductivity values up to 4000 S/cm and electrical failure strains above 1300% [58]. Demonstrations included brain surface interfaces, optoelectronics, and sciatic-nerve stimulators. Although these applications require separate functional assessments, the common design advantage is the incorporation of dimensional control into both supporting and conducting regions. This reduces reliance on a surface treatment to stabilize an otherwise swelling-prone structure.

Dimensional stability alone does not describe how an interface transfers forces to tissue over time. Hydrogels with similar equilibrium moduli may differ in stress relaxation and therefore in their response to sustained or repeated loading. In protein-engineered hydrogels, independently increasing the rate of stress relaxation promoted neurite extension and maturation of human induced-pluripotent-stem-cell-derived neural progenitors [59]. Although this nonconductive in vitro model does not establish electrode performance, it supports considering viscoelasticity alongside softness. Stress–relaxation behavior and storage and loss moduli should be measured at the stated temperature, hydration, and loading frequency, because a low modulus under slow testing may not describe the response during insertion or brain micromotion.

Stable mechanics must be accompanied by reliable attachment between the hydrogel and the underlying electrode. Repeated hydration and deformation can otherwise separate the coating from its substrate, disrupting conduction even when the hydrogel itself remains intact. Laser processing reinforced wet adhesion in PEDOT hydrogels, producing a wet conductivity of 101.4 S/cm, peel strength of 64.4 N/m, and lap-shear strength of 62.1 kPa [60]. Electrochemical properties were retained after one hour of ultrasonication and eight months in water, while brain and cardiac recording demonstrations extended over three weeks. These tests examine different aspects of durability: ultrasonication challenges attachment, soaking examines aqueous stability, and implantation adds tissue remodeling, electrochemical bias, and micromotion. Together, they provide a broader assessment than any single test, without establishing an equivalent lifetime across conditions.

Attachment to tissue presents a related but distinct design problem. Adhesion must be sufficient to prevent gaps and sliding, yet compatible with cortical deformation and, where required, atraumatic removal. A non-deformable adhesive hydrogel patch established wet-tissue adhesion within thirty seconds while addressing both swelling and shrinkage during cortical surface integration [61]. An antifouling network combining dopamine-grafted alginate and poly(ethylene imine) (PEI) further integrated adhesion with dural-defect sealing and gap filling; incorporation into a 128-channel micro-ECoG (μECoG) mesh supported recording over three weeks [62]. These approaches show that tissue attachment can serve structural and barrier functions as well as stabilize recording. Their longer-term value will depend on whether dimensional stability, barrier integrity, and tissue compatibility are maintained together.

The thickness of the tissue-facing layer is equally important, because a protective coating can alter the electrical information reaching the array. An adhesive hydrogel interface was optimized at approximately 10 μm thickness and 2 S/m conductivity, whereas 100-μm layers attenuated functional signals and broadened their spatial spread [63]. For a 64-channel array, the predicted steady-state visually evoked potential (SSVEP) SNR was 94.8% of baseline at sixteen weeks, while uncoated controls showed a larger, nonlinear decline. The result illustrates a trade-off between interfacial protection and signal transmission: increasing coating thickness is not necessarily beneficial, even without changing its chemistry. Spatial filtering and transport distance should therefore be evaluated alongside tissue responses, and separate high-density design validation should remain distinct from the channel configuration used in chronic experiments.

Combining conduction, adhesion, and antifouling behavior within one formulation may simplify contact with irregular tissue surfaces. A photopatternable hydrogel developed for neural interfacing combined conductivity of approximately 6 S/cm, a modulus of 7.25 kPa, and interfacial toughness of approximately 100 J/m^2 [64]. A later injectable adhesive system established stable coupling to fine peripheral nerves; its material impedance remained approximately 120 Ω at 1 kHz after four weeks in PBS at 37 °C, with a separate

four-week vagus-nerve implantation assessment [65]. These results support conformal and durable contact strategies, although performance remains dependent on the anatomical site and assembled device. Material impedance in PBS does not describe the complete implanted cuff, and peripheral-nerve findings do not establish equivalent behavior beneath the dura or within cortical tissue.

Resistance to repeated deformation is another requirement that cannot be inferred from a large one-time stretch. Aligned carbon nanotubes (CNTs) in PVA hydrogel fibers produced spinal microelectrodes approximately 187 ± 13 μm in diameter, with fatigue testing extending to 20,000 cycles at 20% strain [66]. An approximately 1.8 μm SEBS coating insulated the fiber while leaving recording regions selectively exposed. Reinforcement can also be directed at the conductor–substrate boundary: nanocrystalline domains introduced at a conducting-hydrogel/metal interface resisted fatigue cracking and delamination during repeated volume changes [67]. The spinal and muscular experiments in the former study and the cardiac-pacing demonstration in the latter support these mechanical strategies, while validation for brain implantation requires the relevant loading and tissue environment. Accelerated aging in artificial cerebrospinal fluid likewise remains distinct from the duration of functional in vivo recording.

Patterned encapsulation can leave the conductive hydrogel exposed at recording and stimulation sites, preserving ionic access, while a continuous moisture barrier covers the interconnects and electrical junctions to limit fluid ingress and leakage. The seal around each opening must remain intact as the hydrogel swells and the device deforms. In the CHIP array, openings in the Parylene encapsulation exposed the active electrode sites while the connecting traces remained insulated [46]. For all-hydrogel arrays that use hydrated encapsulation layers [44], channel isolation and resistance to fluid ingress should be evaluated separately under prolonged hydration.

Barrier defects become particularly consequential when chemical, electrical, and mechanical stresses act together. Thin-film neuromodulation electrodes exposed to stimulation, hydrogen peroxide, agitation, and elevated temperature over three months showed delamination and gold corrosion as major failure modes; protection by PEDOT depended on its overlap with the underlying metal [68]. Although this study involved films rather than hydrogel electrodes, it explains why initial impedance and soaking stability are insufficient measures of reliability. In a hydrogel device, electrolyte entering through a poorly bonded barrier could corrode a buried conductor or cause leakage while the tissue-facing gel remains intact. Testing should therefore examine physiological soaking, accelerated aging, stimulation, and fatigue separately before assessing their combined effects, with measurements covering both active sites and protected interconnects.

Encapsulation research provides methods for investigating these less visible failure processes. Electrical accelerated aging of amorphous silicon carbide films linked leakage to defect-driven failure and used Weibull analysis to evaluate acceleration [69]. Plasma-treated, silicone-encapsulated complementary metal–oxide–semiconductor (CMOS) structures were also tested in saline under electrical bias at 47, 67, and 87 °C for up to 4.3 years [70]. These studies emphasize defect control, surface preparation, and electrical bias, but their results cannot be transferred directly to a conductive-hydrogel laminate. Estimating physiological lifetime from elevated-temperature testing requires a validated acceleration model and evidence that the failure mechanism remains consistent.

The challenge is therefore to introduce effective barriers without sacrificing the compliance of the hydrated interface. For a rectangular layer of fixed width, bending stiffness scales with elastic modulus and the cube of thickness; in a laminate, each layer's distance from the neutral plane also contributes. A thin, stiff barrier may thus have a modest effect on

bending resistance, whereas a soft coating on a thick, rigid shank may leave overall stiffness largely unchanged. Barrier selection should therefore account for the bending behavior and interfacial integrity of the assembled laminate [46,69,70]. Measurements before and after the intended sterilization process can identify changes in swelling, wet adhesion, and electrical performance (Section 5.3). During prolonged soaking in a physiologically relevant fluid, cyclic deformation representative of the implant site can be used to challenge the encapsulation. Active-site impedance should be tracked separately from leakage current and interchannel isolation, and the edges of the openings and the interfaces between layers should be inspected for cracks or delamination. Accelerated aging can help identify failure modes, which should be compared with those observed during long-term soaking under physiological conditions.

Chemical stability and safety similarly depend on the processed formulation rather than the nominal identity of its components. Removing excess leachable PSS before blending PEDOT with polyurethane improved the viability of L929 and U87 cultures exposed to composite extracts, without significantly changing impedance at 1 kHz or charge storage capacity [71]. Although this conductive-elastomer study does not establish chronic brain compatibility, it demonstrates that processing can alter biological responses without sacrificing the measured electrical properties. Residual monomers, crosslinkers, solvents, and released conductors should therefore be assessed in the final formulation, including after aging, with extract tests complemented by tissue-specific implantation evidence. Degradable devices require an additional distinction between functional duration and biological follow-up. MXene-hydrogel devices supported muscle recording over five days, while degradation and tissue tolerance were assessed separately over eight weeks after implantation in rat muscle [72]. Such peripheral evidence supports transient conducting networks, but brain-specific inflammation, transformation products, and clearance remain to be established.

Interfacial reliability is best assessed by following the complete device from equilibration through use to failure. Impedance spectra, leakage, recording quality, and stimulation charge delivery should be tracked alongside adhesion, dimensional changes, and tissue outcomes. Charge storage capacity (CSC), derived from voltammetry, and charge injection capacity (CIC), determined under a specified stimulation pulse, describe different properties and require separate test conditions. Electrical deterioration also needs to be traced to its source, since dehydration, delamination, and insulation defects can produce changes resembling those associated with inflammation [46,60,63,69,70].

The most promising material strategies differ according to the demands of each interface (Tables 2 and 3). For scalp EEG, compliant semidry gels that retain electrolytes and bilayers that separate ionic conduction from adhesion to the electrode support are promising for maintaining stable skin contact during wear and movement [39,41,42]. At the cortical surface, ultrathin PEDOT-based arrays and thin, wet-adhesive ionic gels applied over conducting electrodes can promote conformal contact. Here, controlling swelling helps maintain contact, while limiting coating thickness helps preserve the spatial selectivity of recording [46,63]. For penetrating probes, thin conducting-polymer coatings with strong attachment to the shank and limited swelling are promising because they must tolerate insertion and subsequent micromotion without substantially enlarging the probe [47,48,52]. For each application, the relevant comparison is how well the assembled electrode maintains impedance and signal quality over time under comparable hydration, geometry, and test conditions.

Table 2. Electrical properties and measurement conditions of representative hydrogel neural interfaces.

Matrix and Conducting Component Application	Conductivity (S/cm)	Impedance (Test Context)	CSC (mC/cm^2)	CIC (mC/cm^2)	Electrical Test Conditions	Ref.
PVA/AgNW–sponge Human scalp	NR	6–8.5 kΩ (system readout)	NR	NR	Eight-channel semidry system; P7/P8 tracked for 10 h; readout frequency not specified.	[39]
Alginate/PAAm–KCl Human scalp	NR	<150 kΩ (human scalp)	NR	NR	EEG-cap real-time readout during 12 h wear; frequency not specified. Separate bench EIS: <0.25 kΩ at 100–100,000 Hz.	[41]
PAAm/alginate–PEDOT:PSS (CHIP) Cortical surface	235 ± 47 (85.9 wt% water)	15.6 Ω·cm^2 (PBS); 8.9 ± 1.2 kΩ (in vivo)	56	4.9	In-plane σ; Z at 1 kHz. PBS, Pt counter/Ag|AgCl reference; CV ±0.5 V, 100 mV/s. CIC: reported biphasic assay; pulse width not specified in main methods.	[46]
PVA/PTPM ionic aGel + PEDOT:PSS electrode Cortical surface	≈0.02 (2 S/m; ionic)	≈20 → 27 kΩ (d1 → d11; in vivo)	NR	NR	64-channel chronic µECoG; Z at 1 kHz. ≈10-µm aGel over a separate PEDOT:PSS-coated electrode; ionic gel is not a mixed electronic conductor.	[63]
PNIPAM-derived fibers/PT6OMe (NG95PT10) Penetrating: thalamus	NR	7.21 ± 1.35 → 5.05 ± 1.09 kΩ (23 → 37 °C)	NR	NR	Bulk gel discs, Ø1 cm × ≈100 µm; sweep 1 Hz–100 kHz. Frequency of quoted Z values not specified; not implanted-probe impedance.	[50]
Microgel-crosslinked PAAm/LMA + aCSF (HM-2) Penetrating: hippocampus	NR	NR	NR	NR	Ionic gel in PI-coated silica capillary; LFP device OD/ID = 450/320 µm. Spike recording used a different microelectrode configuration.	[49]
PAA/PEDOT:PSS T-ECH; T-ECA adhesive variant Peripheral/cardiac	247	27.8 Ω	80	NR	T-ECH: four-point σ after 24 h equilibration; PBS EIS at 1 kHz, exposed area 3 × 3 mm. CV −0.5 to +0.5 V, 100 mV/s; Ag|AgCl reference.	[29]
Laser-treated PEDOT:PSS Brain/cardiac demonstrations	101.4 (wet)	NR	NR	NR	Pure conducting-polymer hydrogel patterned on polymer substrates; wet conductivity. Reported pattern resolution: 5 µm.	[60]
PEG–MXene/PEDOT:PSS/TA (ICAA) Peripheral vagus nerve	0.9243 ± 0.0765 (92.43 ± 7.65 S/m)	≈120 Ω (after 4 wk)	NR	0.139	PBS-equilibrated four-point σ. Z: 1 kHz, PBS, 37 °C. Gel on Ø3-mm Au; reported injection assay: ±0.5 V biphasic pulses, 1.5 ms.	[65]

Table 2. *Cont.*

Matrix and Conducting Component Application	Conductivity (S/cm)	Impedance (Test Context)	CSC (mC/cm^2)	CIC (mC/cm^2)	Electrical Test Conditions	Ref.
Aligned CNT/PVA fiber Intraspinal; indirect for brain	NR	33.20 ± 9.27 kΩ (1 cm specimen)	NR	NR	1 kHz; Ø187 ± 13 µm fiber after 200% prestretch and 5000 training cycles at 10% strain. Value is for a specimen, not an implanted electrode–tissue Z.	[66]
Ca^{2+}-crosslinked $Ti_3C_2T_x$ MXene; gelatin/PLGA device Acute cortex and PNS	7.90 ± 1.50 (hydrated; 790 ± 150 S/m)	2.27 ± 0.83 kΩ (Ø1 mm)	207.1 ± 48.8 (cathodic)	0.23 ± 0.07	Ø1-mm electrodes; PBS, pH 7.4; Z at 1 kHz, 10 mV RMS. CV −1.3 to +0.5 V vs. Ag|AgCl, 50 mV/s. CIC: 500/200/2000 µs cathodic/gap/anodic; cathodic limit −1.3 V.	[72]

Values refer to the specified composition, hydration state, geometry, and protocol; they do not establish a ranking across applications. NR = no verified numerical value available in the source text examined for the listed configuration; graphical-only values were not digitized. NR does not mean zero or that the property was not studied.

Table 3. Mechanical properties, swelling, adhesion, and durability of representative hydrogel neural interfaces.

System	Modulus (kPa)	Swelling	Adhesion (Test Mode)	Durability and Validation Duration	Mechanical and Stability Test Conditions	Ref.
PVA/AgNW–sponge	E ≈ 58.6 (FEA input)	NR	NR	Human: 3 h BCI task; separate 10 h impedance tracking.	Calculated hydrogel modulus used in contact simulation; 10% relative displacement.	[39]
Alginate/PAAm–KCl	Ec ≈20	NR	Substrate bonding; numeric value NR	Human: 12 h N170 test; reuse over 14 d (2 h/day).	Compression-derived modulus; glycerol-containing gel. Adhesion layer bonds gel to electrode support.	[41]
CHIP	Egel = 780 ± 60; Earray = 61,300	Swelling ratio NR; in-plane expansion constrained	NR	Bench: >100 d in PBS; 10,000 CV cycles (<1% CSC change). Rabbit ECoG: longest 550 d.	Gel modulus at 85.9 wt% water; effective array modulus for 9-µm laminate. Chronic recording sampled every 15 d.	[46]
PVA/PTPM aGel	E = 109.4 ± 19.5	Δm/m0: 143.8 ± 6.3%; ΔV/V0: 118.1 ± 11.9%	25.2 ± 3.8 kPa (tissue lap shear)	Bench: 1 month in PBS; 100 d at 60 °C (aging). Rat ECoG: 16 wk; Predicted SSVEP SNR retention: 94.8%.	Swelling relative to dry gel; 1× PBS, pH 7.4, RT, 180 min. Aging duration is not an in vivo lifetime.	[63]

Table 3. *Cont.*

System	Modulus (kPa)	Swelling	Adhesion (Test Mode)	Durability and Validation Duration	Mechanical and Stability Test Conditions	Ref.
NG95PT10	G′ = 10.9 ± 0.14	Thermal deswelling at 37 °C; ratio NR	NR	Bench impedance: 10 d. Mouse thalamus: electrophysiology through 6 wk; spikes declined by week 6.	G′ at 1 Hz, 25 °C, 1% shear strain. G′ is not Young's modulus; recordings at multiple follow-up time points.	[50]
HM-2 ionic gel	E = 59.7	NR	NR	Rat hippocampal CA1: LFP follow-up 4 wk; histology at 1 and 4 wk.	Tensile gel modulus; not the modulus of the capillary-supported device. No quantitative swelling value tabulated.	[49]
T-ECH/T-ECA	E ≈25	NR (water content ≈ 90 wt%)	750 J/m^2 (artery); 250 J/m^2 (kidney) [T-ECA variant]	Bench: 7 d in PBS with stable Z and CSC. Acute peripheral stimulation/cardiac demonstrations.	Tensile strain rate 50%/min. Adhesion: T-ECA, wet tissue, 180° peel; adhesion values are not for unmodified T-ECH.	[29]
Laser-treated PEDOT:PSS	NR	NR	64.4 N/m (peel); 62.1 kPa (lap shear)	Bench: 1 h ultrasonication; 8 months in water. In vivo recording demonstrations: 3 wk.	Wet hydrogel–polymer substrate adhesion. Water storage is distinct from implantation duration.	[60]
ICAA	Et = 32.3 ± 2.9 (high-solids gel)	Δm/m0 = 9.22 ± 0.76%	20.9 kPa (nerve tissue)	Bench: 4 wk in PBS, 37 °C; 100,000 injection cycles. Rat vagus-nerve interface: 4 wk.	Swelling relative to as-prepared gel; PBS, 37 °C, equilibrium ≈24 h. Lap shear: 10 min bonding at 37 °C; 20 mm/min.	[65]
Aligned CNT/PVA	NR	NR	NR	Bench: up to 20,000 cycles at 20% strain; aCSF aging at 45 °C for 5 wk. Separate spinal/muscle recordings.	Cyclic tensile testing of fibers; ≈1.8-µm SEBS insulation in devices. Aging is not a 5-wk in vivo recording claim.	[66]
MXgel	Edevice = 324.8 ± 134.0	Numeric ratio NR	NR	Bench: 1000 bends; 10,000 pulses. Muscle EMG: 5 d; separate muscle degradation/tissue follow-up: 8 wk.	Hydrated laminate after 15 min PBS equilibration. Bending: 20% compression, 20%/s. No chronic cortical duration inferred from muscle follow-up.	[72]

E = Young's/tensile modulus; Ec = compressive modulus; Et = tensile modulus; G′ = shear storage modulus; FEA = finite-element analysis. Mass or volume changes use the explicitly stated baseline. Water content is not a swelling ratio. Peel strength (N/m), lap-shear strength (kPa), and interfacial adhesion energy (J/m^2) are distinct measures. Bench durability, functional recording, and biological follow-up are reported separately.

Against this background, therapeutic functionalization introduces an additional requirement: drug reservoirs and controlled-release pathways must be incorporated without compromising the structural and electrical reliability of the electrode, as discussed in Section 4.

4. Drug Delivery and Therapeutic Functionalization of Conductive Hydrogel Neural Electrodes

Conductive hydrogels can accommodate therapeutic agents within a hydrated electrode–tissue interface, creating opportunities to address biological processes that electrical and mechanical optimization alone cannot resolve. The intended benefit depends on the payload, its local availability, and the extent to which drug delivery can be combined with reliable recording or stimulation. The following discussion is organized around anti-inflammatory and immunomodulatory functions, neurotrophic support and neuroprotection, and the delivery strategies required to implement these functions. Within each subsection, integrated electrode demonstrations are distinguished from material platforms and related delivery technologies that could support future integration. Evidence from spinal cord, peripheral nerve, cochlear, retinal, and wound applications is identified separately because their therapeutic requirements and anatomical environments differ from those of intracortical electrodes.

Therapeutic functionalization combines local drug delivery with electrical interfacing, with distinct spatial arrangements of conductive pathways, drug reservoirs, and release mechanisms supporting anti-inflammatory modulation and neurotrophic delivery (Figure 3).

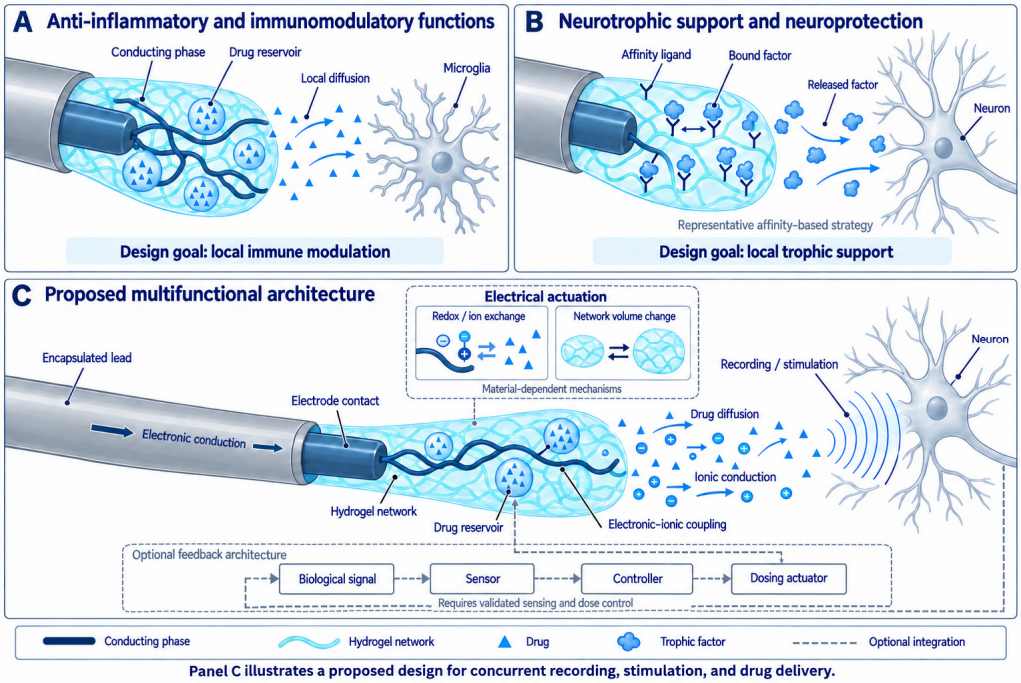


Figure 3. Schematic of drug delivery and therapeutic functions at conductive hydrogel neural interfaces. (**A**) Local anti-inflammatory and immunomodulatory delivery. (**B**) Affinity-based delivery of neurotrophic factors. (**C**) Proposed architecture for concurrent neural recording, electrical stimulation, and controlled drug delivery. The dashed loop indicates an optional feedback pathway that requires validated sensing and dose control.

4.1. Anti-Inflammatory and Immunomodulatory Delivery

Local anti-inflammatory delivery aims to preserve electrode function by limiting the tissue response to implantation. The therapeutic requirements change over time: early treatment targets insertion-related injury, whereas later intervention must address continuing interactions among immune cells, the coating, and the implanted substrate. Combining drug delivery with suitable surface chemistry and mechanics may therefore be more effective than treating these factors independently. One device-level approach incorporated dexamethasone sodium phosphate (DSP) into calcium alginate/chitosan hydrogel coatings alongside platinum nanoparticles and PEDOT modifications for neural activity detection [73]. Another separated the functions into minocycline-loaded polycaprolactone/silk fibroin methacrylate nanofibers, nanostructured PEDOT, and an outer silk fibroin methacrylate hydrogel [18]. The latter supported recording for eight months, while the drug-releasing fibers were designed to address early inflammation. These architectures illustrate how therapeutic and electrical functions can be combined without requiring the drug-bearing region itself to form the conducting network. They also distinguish the treatment window from the period over which electrode performance is maintained.

Incorporating the drug directly into a conducting hydrogel offers a more compact architecture, but couples release to the hydration, mechanical behavior, and degradation of the electrode material. An electrogelated silk/gelatin/reduced graphene oxide (rGO) system containing dexamethasone (DEX) exhibited electrically stimulated, two-stage release together with hydration-dependent mechanical changes and cellular responses relevant to inflammation [74]. This establishes material-level feasibility, although chronic neural recording and the consequences of coating degradation remain unresolved. Across these approaches, the locations of the conductor, drug reservoir, and tissue-contacting layer determine which properties can be adjusted independently and which must be optimized together [18,73,74].

An important question is whether delivery must continue for as long as the electrode remains implanted. Related neural-interface studies suggest that shorter treatment windows can be evaluated against much longer functional outcomes. DEX-loaded carbon nanotubes incorporated into PEDOT coatings enabled electrically triggered delivery during the first 11 days after implantation, while cortical recording was assessed for approximately 540 days [75]. Although not a hydrogel system, this provides a useful example of separating early intervention from long-term device assessment. A different approach used systemically administered, DEX-loaded platelet-inspired nanoparticles, with approximately 65% release within 24 h and 98% within 24 days in vitro, alongside recording assessment over eight weeks [76]. The release profile shows that prolonged delivery can coexist with a substantial initial burst. However, systemic targeting introduces distribution and dosing conditions that differ from those of a coating-bound reservoir.

Extending local exposure requires control over drug retention as well as the amount initially loaded. Chemical attachment can slow release beyond that achieved by physical entrapment alone. DEX covalently attached to polyimide showed cumulative release of 51 ± 15 nmol/cm^2 over nine weeks, with faster release during the first one to two weeks followed by a slower phase [77]. Combining drug retention with a low-fouling surface offers another option. A nonconductive zwitterionic hydrogel on polyimide released $20.47 \pm 3.46\%$ of a 50 μg everolimus load within 8 h and $48.24 \pm 2.45\%$ by day 21, equivalent to 24.12 ± 1.23 μg [78]. These approaches extend therapeutic modification beyond the small recording sites to the surrounding implant surface. Integration with conductive hydrogels would require preserving electrical access, coating adhesion, and drug activity while introducing the retention chemistry.

Drug loading and reservoir structure must also be considered together, because a higher loading does not necessarily produce a higher fractional release. In a cochlear electrode platform, GelMA/MXene/DEX hydrogel was incorporated into porous methacrylated PDMS [79]. During a 40-day test at 37 °C in artificial perilymph, formulations containing 5%, 10%, and 20% DEX released 40.62 ± 0.88%, 35.10 ± 0.13%, and 26.16 ± 3.11% of their payloads, respectively. The 10% formulation was selected as a compromise in release behavior. These percentages must be interpreted alongside the initial drug mass: a lower released fraction at higher loading does not necessarily mean that less drug was delivered. The platform provides an example of hydrogel–electrode integration for antifibrotic delivery, while its cochlear setting differs from the intracortical foreign-body response.

Beyond controlling duration, release may need to respond to changes in the inflammatory environment. Stimulus-responsive and combined immunomodulatory systems developed for spinal cord injury provide relevant design strategies. A bisphosphonate-based hydrogel used the acidic injury environment to promote minocycline release and reduce pro-inflammatory microglial/macrophage responses [80]. Another system combined scavenging of damage-associated molecular patterns with interleukin-10 (IL-10) delivery, targeting both inflammatory signals and downstream cellular responses [81]. These approaches broaden the potential role of a coating from a passive drug depot to a locally responsive interface. Their application to neural electrodes would depend on whether the chemical cues around a chronic implant are sufficient to activate release and whether a much smaller coating reservoir can sustain an effective exposure. Neither study, by itself, demonstrates an integrated conductive hydrogel neural electrode.

Staged delivery offers a complementary way to address changing therapeutic needs without relying entirely on environmental triggers. A dual-drug hyaluronic acid (HA) hydrogel combined minocycline-containing fucoidan nanoparticles with affinity-based retention of interleukin-4 (IL-4) [82]. In the final sequential formulation, minocycline release reached 42.73% at 24 h and 77.73% at seven days, whereas IL-4 release reached 20.19%, 38.76%, and 64.41% at 24 h, seven days, and 30 days, respectively. Both agents were released initially, so the sequence reflected different release timescales rather than a complete transition from one drug to the other. In contrast, a minocycline micelle/thermosensitive gel released 91.25 ± 2.90% within 72 h in pH 7.4 PBS [83]. The contrast illustrates how reservoir design can produce either a relatively short exposure or overlapping delivery phases, depending on the treatment objective.

Taken together, these studies favor matching delivery to the evolving tissue response rather than maximizing release duration alone. Early intervention may be followed by lower or intermittent dosing during subacute remodeling, while prolonged immunomodulation requires evidence of persistent biological dysfunction. For neural electrodes, the central task is to connect local dose and exposure with both tissue outcomes and recording or stimulation performance. This includes determining whether sustained treatment interferes with repair or homeostasis.

Histological evaluation around implanted electrodes should distinguish microglial and macrophage responses, astrocytic reactivity, and neuronal preservation. Ionized calcium-binding adaptor molecule 1 (Iba1) labels both resident microglia and infiltrating macrophages, while cluster of differentiation 68 (CD68) staining helps assess their phagolysosomal response. Determining cell origin or inflammatory phenotype requires additional markers. Glial fibrillary acidic protein (GFAP) immunoreactivity is used to assess astrocytic reactivity, and counts of cells positive for neuronal nuclear antigen (NeuN) estimate local neuronal density. Assessing the function of these neurons re-

quires electrophysiological measurements [7,12,50,76]. Quantifying staining at defined distances from the electrode tract and at selected postimplantation endpoints helps resolve spatial and temporal differences in tissue response. These findings should be interpreted alongside serial measures of electrode impedance, recording signal-to-noise ratio, and active-channel yield. For example, an intracortical electrode study of systemically administered dexamethasone-loaded nanoparticles combined longitudinal recordings with distance-resolved measurements of CD68, GFAP, and NeuN at the eight-week endpoint [76].

4.2. Neurotrophic Support and Neuroprotection

Controlling inflammation is only one part of preserving a functional neural interface. Neurons lost near an implant are not necessarily replaced when inflammation subsides, and surviving neurons may still lose functional connections. Neurotrophic and neuroprotective delivery therefore seeks to maintain neuronal survival and the neural population available for recording or stimulation. For protein therapeutics, this requires preserving biological activity as well as controlling release: the amount recovered from a hydrogel does not necessarily represent the amount capable of producing a cellular response. Current evidence comes largely from neural-repair hydrogels, which offer delivery strategies for electrode integration but rarely demonstrate these functions within a complete, chronically recording conductive hydrogel electrode.

Defined molecular interactions can improve protein incorporation and retention compared with nonspecific physical entrapment. Recombinant spider silk combined with SpyTag/SpyCatcher chemistry enabled functionalization of thermally responsive hydrogels with ciliary neurotrophic factor (CNTF), supporting prolonged Janus kinase (JAK)/signal transducer and activator of transcription 3 (STAT3) signaling, neuronal survival, and axonal regeneration after optic nerve injury [84]. Affinity-based systems provide another way to regulate protein availability. Heparinized poloxamer hydrogels sustained neurotrophin-3 (NT-3) release for 28 days while preserving biological activity [85], and hyaluronic acid–methylfuran hydrogels supported affinity-based NT-3 delivery over 28 days, with released-factor activity verified for at least 14 days [86]. Together, these studies show how molecular binding can support local protein presentation and delivery. They also highlight the need to report release duration and verified bioactivity separately, since the two windows may not coincide.

Retaining an active protein does not, however, ensure that its availability matches the changing needs of injured tissue. Responsive delivery offers a way to link release to local biological conditions. A matrix metalloproteinase (MMP)-responsive conductive hydrogel released basic fibroblast growth factor in the spinal cord injury environment while providing mechanical and electrical properties intended to support repair [87]. Modular, egg-like nanoparticles incorporated into collagen hydrogels provided a different route to spatiotemporal regulation, using internal and external stimuli to control delivery during spinal cord repair [88]. These approaches extend control beyond a predetermined release schedule, although their transfer to chronic electrodes requires defining the relevant trigger range, reproducibility, and persistence of protein activity. The conductive system demonstrates the coexistence of conduction and therapeutic delivery, rather than the recording or stimulation performance of an implanted electrode.

Combining neurotrophic delivery with a conducting network is also supported by peripheral nerve repair studies. Conductive hydrogels containing acrylic acid derivatives, gelatin, and heparin were used to deliver nerve growth factor (NGF) across a 10 mm sciatic nerve defect, with functional, electrophysiological, and histological assessments supporting the repair strategy [89]. Small molecules offer an alternative to protein payloads.

Methylcobalamin incorporated into PEDOT/HA hydrogels was combined with electrical stimulation for peripheral nerve regeneration; release was faster during the first six days and continued more slowly from days 6 to 11 [90]. The reported cumulative release concentration exceeded 100 µM during the first two days, but this value describes the release medium rather than the concentration achieved in nerve tissue. These examples establish useful material functions, while leaving local tissue exposure and stable brain-electrode operation as separate questions.

More complex repair systems combine therapeutic delivery with cells or multiple agents to address several biological processes. An injectable, self-healing conductive hydrogel containing neural stem cells and donepezil released approximately 75% of the drug by day eight and supported local treatment of spinal cord injury [91]. Because the cells, drug, and conducting matrix contributed together, the repair outcome cannot be attributed to release kinetics alone. Staging complementary agents offers another strategy. A dual-phase silk fibroin methacrylate (SilMA) scaffold combined angiotensin-(1–7) (Ang-(1–7)) with NT-3-loaded poly(lactic-co-glycolic acid) (PLGA) microspheres [92]. More than 40% of Ang-(1–7) was released within three days and nearly all within seven days, while approximately 14% of the NT-3 payload was additionally released between days 28 and 56. Although nonconductive, this scaffold illustrates how early microenvironment modulation can be paired with longer neurotrophic delivery. The different release timescales do not imply that inflammation and regeneration occur as independent biological phases.

Evidence from sensory neural tissues further shows why reservoir persistence, protein release, and therapeutic activity must be evaluated separately. A thermosensitive hydrogel containing brain-derived neurotrophic factor (BDNF)-loaded PLGA particles remained in the middle ear for two weeks and improved hearing and cochlear synaptic outcomes after noise-induced injury [93]. This establishes local retention and biological benefit, but residence time alone does not define how long an effective BDNF concentration was maintained. Similarly, a thermosensitive hydrogel containing CNTF and triamcinolone acetonide increased retinal ganglion cell survival at day 28 to 31.05 ± 1.41%, compared with 16.79 ± 1.50% in controls [94]. Its hydrophilic-protein release experiment used bovine serum albumin (BSA), however, so the resulting curve cannot be taken as a direct measurement of CNTF release. Carrier comparisons must account for such differences, particularly when proteins vary in binding affinity and susceptibility to degradation.

Longer retention is therefore a means of controlling exposure, rather than evidence of therapeutic success in itself. An intrathecally administered NT-3 hydrogel remained alongside the rat spinal cord for at least seven days, yet produced no clear improvement in functional recovery or tissue regeneration [95]. This finding underscores the importance of selecting the appropriate factor, active concentration, anatomical distribution, and exposure period. For neural-electrode integration, these variables need to be related to neuronal survival and recording or stimulation performance, including whether prolonged neurotrophic signaling changes excitability or connectivity within the monitored circuit. The objective is to establish an effective therapeutic window within a functioning interface, rather than simply to achieve the longest release duration. Representative systems and their release characteristics, follow-up periods, and levels of integration are compared in Table 4.

Table 4. Representative drug-delivery systems relevant to conductive hydrogel neural electrodes.

Study and System	Evidence and Site	Release Profile/Dose	Release Test Window	In Vivo Follow-Up	Electrical Endpoint	Biological Outcome	Ref.
Bansal 2022 GelMA/PPy; glutamate	Direct Matrix In vitro	≈5× passive release (−0.6 V)	—	NA	Stable over 1000 CV cycles; CSC increased	Cytocompatible extracts	[96]
Qu 2024 Conductive IPN microneedles; GABA/VPA	Direct Matrix Brain	GABA: ≈77.55% after 50 triggers; <5% passive leakage at 10 d	50 triggers; 10 d passive test	4 wk tissue assessment	Neural recording coupled to feedback dosing	Seizure suppression; limited tissue response	[51]
Wang 2025 CA/CS–DSP coating with PtNP/PEDOT:PSS	Indirect [1] Device-level Brain	DSP profile: —	—	—	Spikes/LFPs and dopamine detection	Improved interface biocompatibility	[73]
Pang 2025 MH nanofibers/PEDOT/SFMA hydrogel	Indirect [1] Layered device Brain	Early MH release; curve in Figure S10 in the Supporting Information of Ref. [18]	—	8 mo recording; 1 and 4 wk histology	38.6 ± 2.6 kΩ (1 kHz, PBS); SNR ≈ 20	Reduced astroglial response; neuronal preservation	[18]
Golabchi 2025 PEDOT/CNT–DEX film	Indirect No hydrogel Brain	Electrically triggered DEX delivery	11 d dosing schedule [2]	540 d recording	Improved chronic recording stability	Tissue outcome: —	[75]
Li 2025 DEX-loaded platelet-inspired nanoparticles	Indirect Systemic carrier Brain	≈65% at 24 h; ≈98% at 24 d	24 d in vitro	8 wk recording	Higher active-electrode yield	Higher neuronal density; less neuroinflammation	[76]
Turrin 2025 DEX covalently bound to PI	Indirect No hydrogel Peripheral nerve	51 ± 15 nmol/cm^2 cumulative; faster first 1–2 wk	9 wk in vitro	2 and 8 wk tissue assessment	—	Reduced peri-implant fibrotic capsule	[77]
Gori 2022 Zwitterionic hydrogel/PI; everolimus	Indirect Nonconductive gel In vitro	50 µg loaded; 20.47 ± 3.46% at 8 h; 48.24 ± 2.45% at 21 d	>1 mo in vitro	NA	NA	Low fouling; cytocompatibility; release feasibility	[78]
Ren 2025 GelMA/MXene/DEX in porous MA-PDMS	Indirect Other neural site Cochlea	35.10 ± 0.13% at 40 d (10% DEX formulation)	40 d in vitro	28 d auditory/tissue assessment	—	Less basal-turn fibrosis; SGN preservation	[79]

Table 4. *Cont.*

Study and System	Evidence and Site	Release Profile/Dose	Release Test Window	In Vivo Follow-Up	Electrical Endpoint	Biological Outcome	Ref.
Ramos Ferrer 2024 HA-mF hydrogel; NT-3	Indirect Nonconductive gel In vitro	Affinity-based NT-3 delivery	28 d in vitro	NA	NA	Released NT-3 bioactive ≥14 d	[86]
Liu 2025 PEDOT:PSS/HA; methylcobalamin	Indirect Gel without electrode Peripheral nerve	Cumulative medium concentration > 100 μM by 2 d [3]	11 d in vitro	4 wk repair assessment	CMAP recovery; not BCI recording	Improved nerve/myelin repair with ES	[90]
Liu 2023 PANI-based gel; donepezil + NSCs	Indirect Gel without electrode Spinal cord	≈75% at 8 d; no marked initial burst reported	8 d in vitro	6 wk repair assessment	Evoked spinal responses; not BCI recording	BBB score ≈ 10; NSC/drug combination	[91]
Zhang 2024 SilMA; Ang-(1–7) + NT-3/PLGA	Indirect Nonconductive gel Spinal cord	Ang-(1–7): >40% at 3 d, near-complete at 7 d; NT-3: ≈14% additional release at 28–56 d	Ang: 7 d; NT-3: 56 d	8 wk repair assessment	—	BMS ≈ 6; less glial scarring	[92]
Aycan 2023 HA/MA-rGO-PANI; ibuprofen	Indirect Delivery material In vitro	At 140 min: ≈35%, 60%, 86% at 0, 1, 3 V, respectively	140 min voltage comparison	NA	Conductive gel; no neural recording validation	In vitro cytocompatibility	[97]
Yoon 2022 Microfluidic probe + electrolytic pump	Indirect No hydrogel Brain	0.31–1.15 μL/min; volume within 7% of initial value over 7 d (bench)	7 d bench repeatability	5 d in vivo infusion checks	Concurrent electrophysiology	Localized pharmacological modulation	[98]

[1] The drug-bearing and conducting functions are provided by distinct components of the electrode system. [2] The 11-day interval refers to the stimulation schedule used to trigger dexamethasone release. [3] The reported concentration refers to the in vitro release medium.

4.3. Drug Delivery Strategies and Functional Integration

Effective drug delivery from a neural electrode depends on how the payload is retained, released, and coordinated with electrical operation. Loading strategies and release-control mechanisms address different aspects of this process. Direct incorporation, nanoparticle encapsulation, and affinity retention determine how the drug is accommodated within the coating, whereas electrical actuation and stimulus-responsive networks regulate its availability. Combining these approaches can provide greater control than either alone. An interpenetrating GelMA/PPy hydrogel patterned onto electrodes released approximately five times more glutamate under constant reduction at −0.6 V than without stimulation [96]. This in vitro demonstration established electrically responsive delivery from a conducting hydrogel electrode, providing a starting point for integrating chemical and electrical functions.

Translating triggered release into predictable dosing requires accounting for reservoir depletion. Conductive hydrogel microneedles combining neural recording with antiepileptic delivery achieved cumulative release of approximately 77.55% after 50 cycles of 200 mV, three-minute triggers, while untriggered release remained below 5% over ten days [51]. However, the amount released per cycle declined as the reservoir was depleted, so a fixed electrical command did not produce a constant dose. The platform also incorporated neural feedback and microfluidic replenishment, demonstrating that hydrogel reservoirs can be combined with active fluidic supply. Its extension to anti-inflammatory or neurotrophic delivery would require payload-specific calibration, particularly where binding, transport, and biological activity differ from those of the demonstrated drugs.

For passive delivery, selecting a loading method involves balancing fabrication simplicity against control over retention and release. Direct incorporation requires fewer processing steps but leaves release closely dependent on drug solubility, network mesh size, and drug–matrix interactions. Nanoparticle encapsulation introduces an additional transport barrier that may protect the payload and separate its release from diffusion through the surrounding hydrogel. The minocycline micelle/gel and NT-3 microsphere/scaffold systems illustrate the different delivery timescales achievable through such structures [83,92]. These advantages come with additional processing and possible changes in porosity or mechanics. Affinity retention offers prolonged delivery without a particulate carrier, as demonstrated for NT-3 and IL-4 [82,85,86], although strong binding may leave some of the payload unavailable. The useful loading capacity should therefore be judged by the mass retained after fabrication, the fraction that can be released, and the activity of the released drug.

Electrical actuation adds temporal control but remains dependent on the interactions between the payload and the conducting network. A methacrylated HA/rGO/polyaniline (PANI) hydrogel released approximately 35%, 60%, and 86% of its ibuprofen after 140 min at 0, 1, and 3 V, respectively [97]. For hydrophobic-drug incorporation, hierarchically structured carboxymethyl-hexanoyl chitosan (CHC)-doped PEDOT/silk hydrogels achieved ibuprofen encapsulation efficiency above 90% and were integrated into an electrically controlled wound patch [99]. Electrically modulated noncovalent interactions provided another release mechanism, producing 39–48% guest release within 120 min at 1.5 V, with a release threshold of 0.5 V [100]. These examples demonstrate different routes to electrically regulated delivery, but their performance metrics are not interchangeable. Encapsulation efficiency measures the proportion of initially supplied drug retained during loading, rather than its mass fraction in the hydrogel or its subsequent released fraction. Similarly, voltages used in material-level release assays require separate assessment before application at a neural interface.

The material changes that enable drug release can also affect electrode performance. For example, electrochemical doping of the glycolated polythiophene p(g3T2) produced reversible volume changes of up to 300%, enabling the loading and release of molecules including insulin [101]. In a drug-releasing electrode, charged payloads may affect counterion exchange and the doping state of the conducting polymer. Changes in hydration and swelling during loading or release can also alter ionic conductivity and electrode–electrolyte impedance [51,96,97,101]. For neural recording, these effects can be assessed by measuring impedance across the recording frequency band alongside baseline noise and signal-to-noise ratio. For stimulation, charge storage capacity (CSC) reflects the charge accessed during a voltammetric scan, while charge injection capacity (CIC) should be determined separately from voltage transients under a specified biphasic pulse and electrode polarization limit [36]. A matched unloaded electrode helps isolate the contribution of the drug. For instance, incorporating PPy and glutamate into GelMA increased CSC [96]. Determining the contribution of glutamate would require comparison with a GelMA/PPy coating prepared without glutamate. More generally, loaded and unloaded electrodes should be matched in geometry, base formulation, and electrical exposure, using an empty carrier in the control when applicable. Impedance, CSC, and CIC should be compared at baseline and after defined release intervals, with the released drug mass measured in parallel. Tracking drift in these measures and inspecting coating integrity after repeated actuation or stimulation would help establish electrochemical stability. Separate actuation sites or fluidic channels may reduce interference, although their effectiveness must be established in the complete device.

Meaningful comparison of drug-release behavior requires the absolute amount released, release rate, and initial burst to be reported under clearly defined testing conditions. Diffusion-based and empirical models, including Higuchi and Korsmeyer–Peppas, can help describe release profiles and compare formulations. Such approaches have also been explored for surface-bound DEX [77]. Their interpretation must nevertheless account for material structure and release conditions, since a good fit alone cannot establish the underlying mechanism. This is particularly relevant to conductive hydrogels, where swelling, bond cleavage, and electrical actuation may alter drug transport during release.

A cumulative release curve describes how much drug enters the test medium over time. To assess therapeutic efficacy, it is also necessary to determine how much active drug reaches the target neural tissue and whether it produces the intended biological response. Local concentrations can vary with distance from the electrode and with time after release. An initial burst can produce a brief peak near the implant and leave less drug available later. As the reservoir is depleted, the dose per trigger can decline even under an unchanged actuation protocol, as observed in GABA-releasing hydrogel microneedles [51]. A low release rate at later time points may therefore extend the measured release period while providing little drug during the intended treatment window. For protein payloads, release measurements should be paired with functional assays, such as the axonal growth assays used to verify the activity of released NT-3 [86]. Where feasible, local drug concentrations at defined distances and time points should be related to tissue responses and to recording or stimulation outcomes.

Reservoir capacity places a further limit on coating-based delivery. A thicker coating can hold more drug, but also increases diffusion distance and tissue displacement; a thinner coating may preserve electrical contact while becoming depleted before the therapeutic need has passed. Active transport offers ways to improve distribution without depending entirely on passive diffusion. Combining a hydrogel reservoir with electrokinetic convection-enhanced delivery increased the in vivo penetration distance to 0.88 ± 0.11 mm at 50 µA for 30 min, compared with 0.39 ± 0.11 mm for diffusion alone, using 10% of peak fluorescence to define the distance [102]. These tracer measurements demonstrate enhanced distribution

rather than an effective therapeutic concentration. Mariello et al. used laser-patterned PEDOT:PSS/Au interdigitated electrodes to drive an electroosmotic micropump, achieving an in vitro flow rate of approximately 0.5 nL/min. They also tested a flexible probe prototype in an agarose phantom [103]. This proof of concept illustrates how a dedicated electrical actuator could drive fluid delivery in a flexible neural interface.

Pressure-driven microfluidics addresses the capacity constraint by moving the main reservoir away from the electrode interface and allowing replenishment. A wireless neural probe combining bidirectional delivery with electrophysiology achieved mean flow rates of 1.15, 0.55, and 0.31 µL/min under different actuation schedules, with delivered volume remaining within 7% of its initial value during seven-day testing [98]. A later soft neural interface incorporated a tapered peristaltic micropump for wireless delivery, extending the available compliant fluidic designs [104]. Compared with passive hydrogel coatings, these systems offer more direct control of infusion timing and access to larger or replaceable reservoirs. Their integration requires pumps, connections, and fluidic paths, while actual tissue dosing remains sensitive to backpressure, residual flow, and channel patency. Temporal performance should therefore be assessed at the outlet and through the biological response, rather than inferred solely from pump switching.

A flexible neural probe used 16 recording sites and two dedicated sites for electrically triggered GABA or glutamate release. Separate recording and release circuits and counter electrodes helped reduce actuation artifacts [105]. Conductive hydrogel microneedles have also demonstrated neural activity-triggered drug delivery in vivo [51]. Figure 3C extends these examples to a proposed architecture that also incorporates electrical stimulation. When stimulation and drug release share an electroactive coating, stimulation pulses may alter the polymer redox state and trigger unintended release [36,96]. Dedicated actuation electrodes allow the dosing waveform to be controlled independently. Where the application permits, stimulation and dosing can be scheduled outside recording windows, with recording resumed after the signal recovers. Testing the assembled device should assess unintended release during stimulation, recording recovery after actuation, and electrochemical stability over repeated cycles. Iontronic click-to-release separates transport from payload liberation by pumping a charged trigger that subsequently releases a tethered molecule [106]. The reported electrochemical transport efficiency of approximately 68% is at +20 nA applied to the tetrazine trigger, not the final therapeutic payload. Such strategies offer additional integration options, but require validation of repeated operation, tissue compatibility, and delivery of the intended drug.

The choice among these strategies ultimately depends on the required level of control. Preset electrical pulses provide programmed delivery, whereas pH- or enzyme-responsive networks provide material-level responsiveness. Closed-loop treatment requires a measured biological state to guide dosing and subsequent adjustment of actuation, as demonstrated by neural-activity-guided antiepileptic delivery from conductive hydrogel microneedles [51]. Impedance may contribute to interface monitoring, but cannot identify inflammation alone because hydration, swelling, delamination, corrosion, and payload depletion can produce similar changes. Chronic therapeutic operation therefore requires validated biological feedback, calibrated dosing, and reliable integration. Protective barriers and adhesion-promoting layers must be evaluated alongside the reservoir, since improved encapsulation may also restrict release or stiffen tissue contact. The central objective is to maintain predictable drug delivery and electrical function together throughout the intended treatment period.

5. Regulatory Considerations for Drug-Releasing Conductive Hydrogels

Drug-releasing conductive hydrogel electrodes combine an electrical interface with local therapeutic delivery. Their evaluation must therefore address not only electrode

performance but also drug quality, exposure, and interactions between the drug and device. The applicable regulatory pathway depends on the intended use, product configuration, and contribution of each constituent to the clinical effect. These considerations should inform material development early, because changes that improve conductivity, release, or tissue contact may also affect manufacturing consistency and safety.

5.1. Regulatory Requirements in China

In China, the regulatory pathway begins with determining the product's management attribute. Under the NMPA Announcement on Matters Concerning the Registration of Drug–Device Combination Products (No. 52 of 2021), combination products follow the drug or medical-device registration pathway according to their primary mode of action [107]. Where the management attribute cannot be determined, applicants should seek formal attribute determination before registration. For a drug-releasing electrode, this requires explaining how the electrical interface and pharmacologically active constituent contribute to the intended clinical benefit, rather than assigning a pathway from the hydrogel composition alone.

Device classification is a separate question. The NMPA guidance issued in June 2026 assigns invasive/implantable BCI medical devices within its scope to class III, with classification code 12-00 [108]. Its scope does not encompass every neural recording or stimulation device, so applicability should be established before the classification is adopted. A system-level example is the implantable BCI hand motor-function compensation system approved in March 2026. It combines an epidural electrode interface, wireless power and communication, and a pneumatic glove to assist grasping in patients with cervical spinal cord injury [109]. This approval illustrates evaluation of an integrated BCI system; it does not establish a regulatory precedent for drug-releasing conductive hydrogels.

For products whose primary action is that of a medical device, Chinese registration-review guidance addresses the safety and effectiveness of the combination as a whole, including risks arising from drug–device interactions [110]. The accompanying guidance on drug identification, quantification, and in vitro release provides a basis for characterizing the drug constituent and its delivery behavior [111]. Applied to conductive hydrogel electrodes, these principles support linking drug content and release to coating integrity and electrical performance. The specific tests and acceptance criteria should reflect the formulation, intended exposure, and identified risks, rather than a uniform checklist for all drug-containing coatings.

Biological evaluation similarly needs to address the finished product and its actual contact conditions. GB/T 16886.1-2022 places biological evaluation within a risk-management process that considers composition, manufacturing, contact site, and contact duration [112]. For chronically implanted brain interfaces, relevant questions extend beyond cytotoxicity to local tissue responses, neuronal preservation, degradation products, and exposure to released constituents. Conductive fillers and therapeutic agents introduce additional variables, including migration, depletion, and changes after sterilization or aging. These risks are best considered together with the performance of the assembled electrode.

Manufacturing consistency connects these regulatory questions to material design. Variations in crosslinking, conductive-component distribution, drug loading, coating thickness, or storage may affect both release and impedance. Development should therefore identify the material attributes and process parameters that control the finished product's performance. Appropriate specifications may include drug identity and content, release behavior, coating integrity, and electrochemical properties, supported by biological evaluation and stability studies proportionate to the intended use.

5.2. Regulatory Requirements in the United States and European Union

In the United States, assignment of a combination product to a lead FDA center is generally based on its primary mode of action (PMOA). Under 21 CFR Part 3, this is the single mode of action providing the most important therapeutic action of the combination product [113]. FDA guidance further explains the role of PMOA in determining regulatory jurisdiction [114]. An electrode component does not automatically establish a device-led pathway, and designation to a device center does not remove the need to assess the drug constituent. Where jurisdiction or classification is uncertain, the FDA Office of Combination Products provides procedures for obtaining an agency determination.

For implanted BCIs intended for patients with paralysis or amputation, FDA guidance provides recommendations for nonclinical testing and the design of feasibility and pivotal clinical studies [115]. Its relevance lies in evaluating the complete system, including electrode reliability, implantation risks, stimulation safety where applicable, and clinically meaningful outcomes. Applicability to a particular drug-releasing electrode depends on its intended use and submission pathway. FDA guidance on ISO 10993-1 provides a complementary risk-based approach to biological evaluation [116]. Neither document supplies a stand-alone approval framework for conductive hydrogels; the evidence package must address the relevant device, drug, and combination-product considerations.

Existing drug-containing electrodes illustrate how these issues persist throughout the product lifecycle. The FDA record for Sprint Quattro Lead (6946M), PMA P920015/S306, dated 24 June 2026, identifies a combination product and concerns a change to stability-testing intervals for steroid-containing cardiac lead families [117]. This is a manufacturing/stability change for existing products, rather than initial approval of a hydrogel electrode. It demonstrates continuing oversight of the drug-containing component, while its cardiac application limits direct comparison with intracranial coatings.

Clinical investigation provides a different type of evidence. In the first-in-human CIDEXEL study, nine participants received a cochlear implant with a FLEX28 DEX array and were followed for up to nine months after first fitting [118]. Safety was assessed alongside electrode impedance, hearing preservation, and speech perception. This study illustrates how electrical measurements can be linked to adverse events and clinically relevant function in a drug-eluting neural electrode. Its intracochlear setting, however, does not establish cerebral safety or demonstrate a conductive hydrogel BCI.

Manufacturing evaluation must also reflect the FDA Quality Management System Regulation (QMSR), effective 2 February 2026. The revised 21 CFR Part 820 incorporates ISO 13485:2016 by reference, with corresponding amendments to combination-product quality-system provisions under 21 CFR Part 4 [119,120]. For hydrogel coatings, this makes control of formulation, suppliers, coating processes, verification, validation, and subsequent changes particularly relevant. A change intended to improve drug retention, for example, may also require assessment of its effects on electrical performance and stability.

In the European Union, Regulation (EU) 2017/745 distinguishes devices incorporating an ancillary medicinal substance from integral products whose principal action is medicinal [121]. Under Article 1(8), products in the former category are assessed under the MDR; Annex VIII, Rule 14 classifies qualifying devices incorporating an ancillary medicinal substance as class III. Where the substance provides the principal action, the applicable medicinal-product framework governs the integral product, while relevant MDR Annex I requirements apply to the device-related safety and performance features.

MDCG 2022-5 Rev. 1 further explains this borderline and the evidence needed to distinguish principal from ancillary medicinal action [122]. For devices incorporating an ancillary medicinal substance, conformity assessment includes consultation with an appropriate medicinal-products authority or the EMA concerning the substance and its incorporation

into the device [123]. The relevant questions are therefore not simply whether adding a drug changes the risk class, but whether it changes the regulatory pathway, introduces consultation requirements, or alters the evidence needed for conformity assessment. These determinations remain product-specific.

5.3. Key Regulatory Evaluation Considerations

For drug-releasing conductive hydrogel electrodes, a central question is whether the therapeutic benefit can be maintained without compromising electrode function. Drug loading may alter network structure and adhesion, while release and depletion can change conductivity and mechanical behavior during use. Evaluation should therefore follow the electrode through these changes rather than rely on its initial properties. Comparisons with drug-free electrodes can help determine whether changes in impedance, recording quality, or tissue response arise from the drug, the coating, or their interaction. The anatomical site and intended duration of use should guide the study design; evidence from skin contact or short-term implantation cannot resolve the risks of chronic brain exposure.

Sterilization and storage can change the same properties that govern delivery and electrical performance. In a study of 30% *w/v* Poloxamer 407, gamma irradiation caused oxidative degradation and cytotoxicity, whereas the tested electron-beam conditions better preserved functional properties [124]. Although the formulation was nonconductive, the result illustrates why a sterilization method must be selected for the finished formulation rather than the polymer alone. For drug-loaded electrodes, comparisons before and after processing should examine drug identity and activity, release behavior, coating integrity, and electrochemical performance. Ethylene oxide additionally requires assessment of residues, while aseptic manufacture depends on validated control of components and assembly. Storage studies should establish whether these properties remain acceptable throughout the proposed shelf life, with real-time data used to support accelerated estimates.

The assembled electrode also needs to be tested because failures often occur between layers rather than within the bulk hydrogel. Comparison of Al_2O_3/Parylene C bilayer encapsulation with Parylene-only encapsulation in Utah-array interfaces demonstrates the importance of evaluating the actual device architecture [125]. In a drug-releasing electrode, the barrier must protect buried conductors while leaving the active interface accessible to ions and drug transport. Leakage, interlayer adhesion, and changes in release after aging are therefore as relevant as the stability of the gel itself. Improving the barrier at the expense of release or tissue conformity would merely shift the source of failure.

Long-term electrical and biological results should be examined together. Rising impedance may accompany inflammation, but can also result from dehydration, delamination, corrosion, or insulation defects. Conversely, stable impedance does not establish safe drug exposure or preservation of nearby neurons. Chronic studies should relate local exposure and tissue responses to sustained recording or stimulation, including performance after the reservoir is depleted. Accelerated soaking and fatigue tests can identify likely failure modes, but cannot replace implantation evidence when tissue interactions are central to the intended use.

Translation thus depends on evidence that the combined functions remain reliable over the required period. Laboratory studies establish material and release behavior; animal investigations examine implantation, exposure, and tissue responses; clinical studies determine safety and meaningful benefit in the intended population. Progress at one stage or in another anatomical application should be interpreted within that scope. The regulatory considerations and relevant experimental evidence are summarized together (Table 5).

Table 5. Regulatory considerations for drug-releasing conductive hydrogel electrodes in China, the US, and the EU.

Evaluation Domain	China	United States	European Union	Corresponding Experimental/Documentary Evidence
Product qualification and classification	Combination-product definition and primary mode of action under No. 52/2021; invasive/implantable BCI devices: class III under 2026 guidance [107,108].	21 CFR Part 3; lead-center assignment based on PMOA; OCP jurisdiction procedures when needed [113,114].	MDR Article 1(8); Rule 14: integral ancillary medicinal substances place qualifying devices in class III [121,122].	Intended use; constituent functions; product architecture; evidence supporting principal action and ancillary benefit. Classification requires individual assessment.
Biological evaluation	GB/T 16886.1-2022 risk-based evaluation [112].	FDA ISO 10993-1 guidance; contact-specific biological evaluation [116].	MDR Annex I biological/chemical safety and risk management [121].	Finished-product characterization; contact site/duration; extractables/leachables, filler migration and degradation products; justified biological endpoints.
Drug characterization	Qualitative/quantitative drug characterization guidance [110,111].	Drug-constituent quality and combination-product interactions [114,120].	Ancillary substance quality/safety/usefulness; medicines-authority consultation [121,123,126].	Identity, content, purity/degradants, uniformity, activity where relevant; local/systemic exposure and dose rationale.
Release and electrical coupling	In vitro release guidance for device-led combinations [111].	Product-specific evidence for release and drug-device interactions [114,120].	Evidence supporting substance quality/safety and incorporation benefit-risk [121,126].	Validated release assay; absolute released mass, burst fraction and depletion; compare release and impedance under intended stimulation and control conditions.
Electrical safety and system function	Device safety/performance evaluation as part of combination review [110].	Implanted BCI guidance: nonclinical testing and clinical study considerations [115].	MDR Annex I active-device safety/performance requirements [121].	Impedance spectrum, recording quality and stimulation safety; insulation/leakage; charge-injection limits where applicable; assembled-system reliability.
Chronic implantation and clinical evidence	Integrated safety/effectiveness evaluation; clinical evidence suited to intended use [108,110].	BCI guidance links preclinical testing with feasibility/pivotal clinical study design [115].	Clinical evaluation and post-market clinical follow-up as applicable [121].	Longitudinal tissue and electrophysiological outcomes; drug-depleted state; justified duration; device failures, adverse events and functional outcomes.
Sterilization and shelf life	Finished-product and manufacturing risks within integrated review [110].	QMSR/Part 4 controls and product-specific validation [119,120].	MDR Annex I infection/contamination controls; QMS conformity assessment [121].	Validated terminal sterilization or aseptic manufacture; residuals as applicable; drug activity, release and electrical/coating properties after processing and storage.
Manufacturing quality control	Control formulation, processing and drug-device interactions [110,111].	QMSR (21 CFR Part 820) and applicable Part 4 requirements [119,120].	MDR Article 10(9), Annexes II/III and conformity assessment [121].	Batch reproducibility of drug content, release, thickness, adhesion and electrical properties; process validation, supplier/change controls and traceability.

6. Conclusions and Outlook

The requirements of the target neural interface guide the choice of hydrogel composition and coating geometry. In a drug-releasing electrode, those same choices also determine how much drug the coating can carry, how it is released, and how the electrode maintains contact with tissue as release proceeds. For implanted electrodes, the main unresolved challenge is therefore to deliver a reproducible, therapeutically relevant local drug exposure while maintaining stable recording or stimulation throughout the intended period of use. Resolving this challenge is central to assessing the safety and performance of the finished electrode.

The first step is to measure drug release and track electrical performance in the same electrode, from initial drug loading through reservoir depletion. For mixed ionic–electronic conductors, high initial conductivity should be complemented by evidence that interfacial charge transfer and recording or stimulation performance remain stable under physiological hydration, repeated electrical operation, and material aging. Drug delivery requires similarly explicit characterization: the loaded and released mass, burst fraction, release rate, retained activity, and duration of effective exposure should be reported wherever measurable. These measurements must be related to changes in swelling, adhesion, impedance, and charge-injection behavior during loading and depletion. Demonstrating prolonged release alone is insufficient if the delivered concentration is ineffective or the release process compromises electrode function.

The next priority is chronic validation using the intended electrode architecture and anatomical setting. Matched drug-free controls and concurrent assessment of electrical function, therapeutic exposure, and tissue responses are needed to determine whether local treatment provides a sustained benefit beyond that of the hydrogel coating itself. Follow-up should extend beyond the release period where relevant, because reservoir exhaustion may precede electrical or biological failure. Standardized reporting of device geometry, test conditions, sterilization, storage, manufacturing variability, and failure criteria would make these studies more comparable and more useful for regulatory assessment. Translation further requires product-specific consideration of intended use, primary mode of action, and constituent interactions; experience with conventional BCIs or other drug-eluting devices cannot substitute for evidence from the finished hydrogel electrode.

Adaptive therapeutic delivery represents a longer-term direction that depends on resolving these foundational issues. Externally programmed release and stimulus-responsive materials should be distinguished from genuine closed-loop systems that combine validated biological sensing, a feedback algorithm, and adaptive dosing. In particular, impedance changes alone cannot establish inflammation or determine a therapeutic dose. Hybrid interfaces combining conductive hydrogels with microfluidic or electroosmotic delivery may improve dosing flexibility, but their potential must be weighed against reservoir, packaging, and integration constraints. Progress should therefore prioritize reproducible integrated operation and chronic safety before advancing to increasingly complex autonomous control.

Author Contributions: J.Z.: Conceptualization, Methodology, Investigation, Data curation, Visualization, Writing—original draft. Y.C.: Investigation, Data curation, Writing—original draft. Y.G. and Q.Y.: Investigation, Literature curation, Writing—original draft. Y.W.: Formal analysis, Investigation, Visualization. C.Z.: Resources, Supervision, Writing—review and editing. H.W.: Conceptualization, Methodology, Supervision, Project administration, Funding acquisition, Writing—review and editing. All authors have read and agreed to the published version of the manuscript.

Funding: This study was supported by the Fundamental Research Funds for the Central Universities (Grant No. 2025JBZX002) and the Key Project for the Development of the Regulatory Science System, "Research on Systematic Evaluation Methods for the Safety and Effectiveness of Medical Devices Based on Brain–Computer Interface Technology" (Grant No. RX2024X007).

Institutional Review Board Statement: Not applicable.

Informed Consent Statement: Not applicable.

Data Availability Statement: No new data were created or analyzed in this review study. Data supporting the findings discussed in this review are available from the corresponding author upon reasonable request.

Acknowledgments: During the preparation of this manuscript, the authors used ChatGPT (OpenAI, GPT-6.1 Sol, San Francisco, CA, USA) for language polishing and English expression improvement. The authors have carefully reviewed and edited the generated content and take full responsibility for the final content of the publication.

Conflicts of Interest: The authors declare no conflicts of interest.

Abbreviations

The following abbreviations are used in this manuscript:

aCSF	Artificial cerebrospinal fluid
AgNW	Silver nanowire
BBB score	Basso–Beattie–Bresnahan locomotor rating scale
BCI	Brain–computer interface
BDNF	Brain-derived neurotrophic factor
BMS	Basso Mouse Scale
BSA	Bovine serum albumin
CA	Calcium alginate
CD68	Cluster of differentiation 68
CE	Conformité Européenne (European conformity)
CFR	Code of Federal Regulations
CHC	Carboxymethyl-hexanoyl chitosan
CIC	Charge injection capacity
CMAP	Compound muscle action potential
CMOS	Complementary metal–oxide–semiconductor
CNT	Carbon nanotube
CNTF	Ciliary neurotrophic factor
CS	Chitosan
CSC	Charge storage capacity
CV	Cyclic voltammetry
DEX	Dexamethasone
DSP	Dexamethasone sodium phosphate
ECoG	Electrocorticography
EEG	Electroencephalography
EIS	Electrochemical impedance spectroscopy
EMA	European Medicines Agency
EMG	Electromyography
ES	Electrical stimulation
EU	European Union
FDA	Food and Drug Administration
FEA	Finite-element analysis
GABA	γ-Aminobutyric acid
GB/T	Recommended national standard of China
GelMA	Gelatin methacrylate
GFAP	Glial fibrillary acidic protein
HA	Hyaluronic acid
HA-mF	Hyaluronic acid–methylfuran
HDE	Humanitarian device exemption
Iba1	Ionized calcium-binding adaptor molecule 1
IDE	Investigational device exemption
IL-10	Interleukin-10
IL-4	Interleukin-4
IPN	Interpenetrating polymer network
ISO	International Organization for Standardization

JAK	Janus kinase
LFP	Local field potential
LMA	Lauryl methacrylate
MA-PDMS	Methacrylated poly(dimethylsiloxane)
MDCG	Medical Device Coordination Group
MDR	Medical Device Regulation (Regulation (EU) 2017/745)
MH	Minocycline hydrochloride
MMP	Matrix metalloproteinase
MXene	Family of two-dimensional transition-metal carbides, nitrides, and carbonitrides
NA	Not applicable
NGF	Nerve growth factor
NMPA	National Medical Products Administration
NR	No verified numerical value available
NSC	Neural stem cell
NT-3	Neurotrophin-3
OCP	Office of Combination Products
OD/ID	Outer diameter/inner diameter
PAA	Poly(acrylic acid)
PAAm	Polyacrylamide
PANI	Polyaniline
PBS	Phosphate-buffered saline
PDMS	Polydimethylsiloxane
PEDOT	Poly(3,4-ethylenedioxythiophene)
PEDOT:PSS	Poly(3,4-ethylenedioxythiophene):polystyrene sulfonate
PEG	Poly(ethylene glycol)
PEI	Poly(ethylene imine)
pHEMA	Poly(2-hydroxyethyl methacrylate)
PI	Polyimide
PLGA	Poly(lactic-co-glycolic acid)
PMA	Premarket approval
PMOA	Primary mode of action
PNIPAM	Poly(N-isopropylacrylamide)
PNS	Peripheral nervous system
PPy	Polypyrrole
pSB	Poly(sulfobetaine methacrylate)
PSS	Polystyrene sulfonate
PT6OMe	Regioregular poly[3-(6-methoxyhexyl)thiophene]
PtNP	Platinum nanoparticle
PTPM	Poly[3-(trimethoxysilyl)propyl methacrylate]
PVA	Poly(vinyl alcohol)
PVP	Poly(vinylpyrrolidone)
QMS	Quality management system
QMSR	Quality Management System Regulation
rGO	Reduced graphene oxide
RMS	Root mean square
RT	Room temperature
SEBS	Poly(styrene-ethylene-butylene-styrene)
SFMA	Silk fibroin methacrylate
SGN	Spiral ganglion neuron
SilMA	Silk fibroin methacrylate
SNR	Signal-to-noise ratio
SSVEP	Steady-state visually evoked potential
STAT3	Signal transducer and activator of transcription 3
TA	Tannic acid
μECoG	Micro-electrocorticography
VPA	Valproic acid

References

1. Hochberg, L.R.; Serruya, M.D.; Friehs, G.M.; Mukand, J.A.; Saleh, M.; Caplan, A.H.; Branner, A.; Chen, D.; Penn, R.D.; Donoghue, J.P. Neuronal ensemble control of prosthetic devices by a human with tetraplegia. *Nature* **2006**, *442*, 164–171. [CrossRef]
2. Hochberg, L.R.; Bacher, D.; Jarosiewicz, B.; Masse, N.Y.; Simeral, J.D.; Vogel, J.; Haddadin, S.; Liu, J.; Cash, S.S.; van der Smagt, P.; et al. Reach and grasp by people with tetraplegia using a neurally controlled robotic arm. *Nature* **2012**, *485*, 372–375. [CrossRef]

3. Willett, F.R.; Avansino, D.T.; Hochberg, L.R.; Henderson, J.M.; Shenoy, K.V. High-performance brain-to-text communication via handwriting. *Nature* **2021**, *593*, 249–254. [CrossRef]
4. Willett, F.R.; Kunz, E.M.; Fan, C.; Avansino, D.T.; Wilson, G.H.; Choi, E.Y.; Kamdar, F.; Glasser, M.F.; Hochberg, L.R.; Druckmann, S.; et al. A high-performance speech neuroprosthesis. *Nature* **2023**, *620*, 1031–1036. [CrossRef]
5. Shih, J.J.; Krusienski, D.J.; Wolpaw, J.R. Brain-computer interfaces in medicine. *Mayo Clin. Proc.* **2012**, *87*, 268–279. [CrossRef]
6. Khodagholy, D.; Gelinas, J.N.; Thesen, T.; Doyle, W.; Devinsky, O.; Malliaras, G.G.; Buzsáki, G. NeuroGrid: Recording action potentials from the surface of the brain. *Nat. Neurosci.* **2015**, *18*, 310–315. [CrossRef]
7. Kozai, T.D.Y.; Jaquins-Gerstl, A.S.; Vazquez, A.L.; Michael, A.C.; Cui, X.T. Brain tissue responses to neural implants impact signal sensitivity and intervention strategies. *ACS Chem. Neurosci.* **2015**, *6*, 48–67. [CrossRef]
8. Fattahi, P.; Yang, G.; Kim, G.; Abidian, M.R. A review of organic and inorganic biomaterials for neural interfaces. *Adv. Mater.* **2014**, *26*, 1846–1885. [CrossRef]
9. Weltman, A.; Yoo, J.; Meng, E. Flexible, penetrating brain probes enabled by advances in polymer microfabrication. *Micromachines* **2016**, *7*, 180. [CrossRef]
10. Polikov, V.S.; Tresco, P.A.; Reichert, W.M. Response of brain tissue to chronically implanted neural electrodes. *J. Neurosci. Methods* **2005**, *148*, 1–18. [CrossRef]
11. Saxena, T.; Karumbaiah, L.; Gaupp, E.A.; Patkar, R.; Patil, K.; Betancur, M.; Stanley, G.B.; Bellamkonda, R.V. The impact of chronic blood-brain barrier breach on intracortical electrode function. *Biomaterials* **2013**, *34*, 4703–4713. [CrossRef]
12. Salatino, J.W.; Ludwig, K.A.; Kozai, T.D.Y.; Purcell, E.K. Glial responses to implanted electrodes in the brain. *Nat. Biomed. Eng.* **2017**, *1*, 862–877. [CrossRef]
13. Yuk, H.; Lu, B.; Zhao, X. Hydrogel bioelectronics. *Chem. Soc. Rev.* **2019**, *48*, 1642–1667. [CrossRef]
14. Cheng, S.; Zhu, R.; Xu, X. Hydrogels for next generation neural interfaces. *Commun. Mater.* **2024**, *5*, 99. [CrossRef]
15. Lu, B.; Yuk, H.; Lin, S.; Jian, N.; Qu, K.; Xu, J.; Zhao, X. Pure PEDOT:PSS hydrogels. *Nat. Commun.* **2019**, *10*, 1043. [CrossRef]
16. Kim, S.; Shin, Y.; Han, J.; Kim, H.J.; Sunwoo, S.H. Introductory review of soft implantable bioelectronics using conductive and functional hydrogels and hydrogel nanocomposites. *Gels* **2024**, *10*, 614. [CrossRef]
17. Kim, D.H.; Martin, D.C. Sustained release of dexamethasone from hydrophilic matrices using PLGA nanoparticles for neural drug delivery. *Biomaterials* **2006**, *27*, 3031–3037. [CrossRef]
18. Pang, J.; Sun, Y.; Cheng, T.; Wang, J.; He, X.; Xiang, Y.; Zhu, W.; Cao, Y.; Wu, M.; Pei, W.; et al. Multifunctional Composite Coating-Enhanced Flexible Microelectrodes for Chronic, High-Fidelity Neural Signal Recording. *Anal. Chem.* **2025**, *97*, 27745–27757. [CrossRef]
19. Gutowski, S.M.; Shoemaker, J.T.; Templeman, K.L.; Wei, Y.; Latour, R.A.; Bellamkonda, R.V.; LaPlaca, M.C.; García, A.J. Protease-degradable PEG-maleimide coating with on-demand release of IL-1Ra to improve tissue response to neural electrodes. *Biomaterials* **2015**, *44*, 55–70. [CrossRef]
20. Politrón-Zepeda, G.A.; Fletes-Vargas, G.; Rodríguez-Rodríguez, R. Injectable hydrogels for nervous tissue repair-A brief review. *Gels* **2024**, *10*, 190. [CrossRef]
21. Shen, C.; Wang, Y.; Yuan, P.; Wei, J.; Bao, J.; Li, Z. Conductive hydrogels in biomedical engineering: Recent advances and a comprehensive review. *Gels* **2026**, *12*, 69. [CrossRef]
22. Sagdic, K.; Fernández-Lavado, E.; Mariello, M.; Akouissi, O.; Lacour, S.P. Hydrogels and conductive hydrogels for implantable bioelectronics. *MRS Bull.* **2023**, *48*, 495–505. [CrossRef]
23. Dawit, H.; Zhao, Y.; Wang, J.; Pei, R. Advances in conductive hydrogels for neural recording and stimulation. *Biomater. Sci.* **2024**, *12*, 2786–2800. [CrossRef]
24. Xue, X.Y.; Han, L.; Cai, H.Q.; Zhang, K.; Sun, Z.C.; Liu, R.P.; Wang, T.H.; Pan, F.H.; Man, W.T.; Wang, D.; et al. Conductive Hydrogel-Based Neural Interfaces: From Fabrication Methods, Properties, to Applications. *Small Struct.* **2025**, *6*, 2400696. [CrossRef]
25. Ghosh, S.; Kumar, N.; Chattopadhyay, S. Electrically conductive "SMART" hydrogels for on-demand drug delivery. *Asian J. Pharm. Sci.* **2025**, *20*, 101007. [CrossRef]
26. Wang, S.; Yu, L.; Wang, S.; Zhang, L.; Chen, L.; Xu, X.; Song, Z.; Liu, H.; Chen, C. Strong, tough, ionic conductive, and freezing-tolerant all-natural hydrogel enabled by cellulose-bentonite coordination interactions. *Nat. Commun.* **2022**, *13*, 3408. [CrossRef]
27. Bansal, M.; Vyas, Y.; Aqrawe, Z.; Raos, B.; Cheah, E.; Montgomery, J.; Wu, Z.; Svirskis, D. Patternable Gelatin Methacrylate/PEDOT/Polystyrene Sulfonate Microelectrode Coatings for Neuronal Recording. *ACS Biomater. Sci. Eng.* **2022**, *8*, 3933–3943. [CrossRef]
28. Li, T.L.; Liu, Y.; Forro, C.; Yang, X.; Beker, L.; Bao, Z.; Cui, B.; Pașca, S.P. Stretchable mesh microelectronics for the biointegration and stimulation of human neural organoids. *Biomaterials* **2022**, *290*, 121825. [CrossRef]
29. Chong, J.; Sung, C.; Nam, K.S.; Kang, T.; Kim, H.; Lee, H.; Park, H.; Park, S.; Kang, J. Highly conductive tissue-like hydrogel interface through template-directed assembly. *Nat. Commun.* **2023**, *14*, 2206. [CrossRef]

30. He, H.; Li, H.; Pu, A.; Li, W.; Ban, K.; Xu, L. Hybrid assembly of polymeric nanofiber network for robust and electronically conductive hydrogels. *Nat. Commun.* **2023**, *14*, 759. [CrossRef]
31. Zhou, T.; Yuk, H.; Hu, F.; Wu, J.; Tian, F.; Roh, H.; Shen, Z.; Gu, G.; Xu, J.; Lu, B.; et al. 3D printable high-performance conducting polymer hydrogel for all-hydrogel bioelectronic interfaces. *Nat. Mater.* **2023**, *22*, 895–902. [CrossRef]
32. Xie, X.; Xu, Z.; Yu, X.; Jiang, H.; Li, H.; Feng, W. Liquid-in-liquid printing of 3D and mechanically tunable conductive hydrogels. *Nat. Commun.* **2023**, *14*, 4289. [CrossRef]
33. Won, D.; Kim, J.; Choi, J.; Kim, H.; Han, S.; Ha, I.; Bang, J.; Kim, K.K.; Lee, Y.; Kim, T.S.; et al. Digital selective transformation and patterning of highly conductive hydrogel bioelectronics by laser-induced phase separation. *Sci. Adv.* **2022**, *8*, eabo3209. [CrossRef]
34. Lu, Y.; Yang, G.; Wang, S.; Zhang, Y.; Jian, Y.; He, L.; Yu, T.; Luo, H.; Kong, D.; Xianyu, Y.; et al. Stretchable graphene–hydrogel interfaces for wearable and implantable bioelectronics. *Nat. Electron.* **2024**, *7*, 51–65. [CrossRef]
35. Zhang, Q.; Lu, H.; Yun, G.; Gong, L.; Chen, Z.; Jin, S.; Du, H.; Jiang, Z.; Li, W. A Laminated Gravity-Driven Liquid Metal-Doped Hydrogel of Unparalleled Toughness and Conductivity. *Adv. Funct. Mater.* **2024**, *34*, 2308113. [CrossRef]
36. Azami, A.; Wu, Y.; Nguyen, C.K.; Abbott, J.R.; Orazem, M.E.; Otto, K.J.; Cogan, S.F.; Kim, B.N. Electrochemical Stability of Electrodeposited PEDOT:PSS Neural Stimulation Electrodes. *Micromachines* **2026**, *17*, 1198. [CrossRef]
37. Li, P.; Sun, W.; Li, J.; Chen, J.P.; Wang, X.; Mei, Z.; Jin, G.; Lei, Y.; Xin, R.; Yang, M.; et al. N-type semiconducting hydrogel. *Science* **2024**, *384*, 557–563. [CrossRef]
38. Dai, Y.; Wai, S.; Li, P.; Shan, N.; Cao, Z.; Li, Y.; Wang, Y.; Liu, Y.; Liu, W.; Tang, K.; et al. Soft hydrogel semiconductors with augmented biointeractive functions. *Science* **2024**, *386*, 431–439. [CrossRef]
39. Liu, J.; Lin, S.; Li, W.; Zhao, Y.; Liu, D.; He, Z.; Wang, D.; Lei, M.; Hong, B.; Wu, H. Ten-Hour Stable Noninvasive Brain-Computer Interface Realized by Semidry Hydrogel-Based Electrodes. *Research* **2022**, *2022*, 9830457. [CrossRef]
40. Han, Q.; Zhang, C.; Guo, T.; Tian, Y.; Song, W.; Lei, J.; Li, Q.; Wang, A.; Zhang, M.; Bai, S.; et al. Hydrogel Nanoarchitectonics of a Flexible and Self-Adhesive Electrode for Long-Term Wireless Electroencephalogram Recording and High-Accuracy Sustained Attention Evaluation. *Adv. Mater.* **2023**, *35*, 2209606. [CrossRef]
41. Xue, H.; Wang, D.; Jin, M.; Gao, H.; Wang, X.; Xia, L.; Li, D.A.; Sun, K.; Wang, H.; Dong, X.; et al. Hydrogel electrodes with conductive and substrate-adhesive layers for noninvasive long-term EEG acquisition. *Microsyst. Nanoeng.* **2023**, *9*, 79. [CrossRef]
42. Su, H.; Mao, L.; Chen, X.; Liu, P.; Pu, J.; Mao, Z.; Fujiwara, T.; Ma, Y.; Mao, X.; Li, T. A Complementary Dual-Mode Ion-Electron Conductive Hydrogel Enables Sustained Conductivity for Prolonged Electroencephalogram Recording. *Adv. Sci.* **2024**, *11*, 2405273. [CrossRef]
43. Wang, X.; Sun, X.; Gan, D.; Soubrier, M.; Chiang, H.Y.; Yan, L.; Li, Y.; Li, J.; Yu, S.; Xia, Y.; et al. Bioadhesive and conductive hydrogel-integrated brain-machine interfaces for conformal and immune-evasive contact with brain tissue. *Matter* **2022**, *5*, 1204–1223. [CrossRef]
44. Zeng, M.; Ding, J.; Tian, Y.; Zhang, Y.; Liu, X.; Chen, Z.; Sun, J.; Wu, C.; Yin, H.; Wei, D.; et al. Dopamine-integrated all-hydrogel multi-electrode arrays for neural activity recording. *Mater. Horiz.* **2024**, *11*, 6423–6434. [CrossRef]
45. Xiang, Y.; He, X.; Cheng, T.; Zhu, W.; Pang, J.; Cao, Y.; Wu, M.; Pei, R.; Cao, Y. A Zwitterionic Conductive Hydrogel Interface for Enhanced Electrocorticography Signal Fidelity via High Conductivity, Antifouling, and Brain-Matched Mechanics. *Biomacromolecules* **2025**, *26*, 7959–7973. [CrossRef]
46. Zhu, R.; Hu, Z.; Lou, Z.; Xie, F.; Zhao, S.; Jiao, X.; Wang, J.; Fukuda, K.; Chen, X.; Hu, W.; et al. An exceptionally conductive hydrogel for all-organic, ultraflexible, and chronic neural interfaces. *Proc. Natl. Acad. Sci. USA* **2026**, *123*, e2532840123. [CrossRef]
47. Zhang, J.; Wang, L.; Xue, Y.; Lei, I.M.; Chen, X.; Zhang, P.; Cai, C.; Liang, X.; Lu, Y.; Liu, J. Engineering Electrodes with Robust Conducting Hydrogel Coating for Neural Recording and Modulation. *Adv. Mater.* **2023**, *35*, 2209324. [CrossRef]
48. Chik, G.K.K.; Xiao, N.; Ji, X.; Tsang, A.C.O.; Leung, G.K.K.; Zhang, S.; Tin, C.; Chan, P.K.L. Flexible Multichannel Neural Probe Developed by Electropolymerization for Localized Stimulation and Sensing. *Adv. Mater. Technol.* **2022**, *7*, 2200143. [CrossRef]
49. Liang, Q.; Xia, X.; Sun, X.; Yu, D.; Huang, X.; Han, G.; Mugo, S.M.; Chen, W.; Zhang, Q. Highly Stretchable Hydrogels as Wearable and Implantable Sensors for Recording Physiological and Brain Neural Signals. *Adv. Sci.* **2022**, *9*, 2201059. [CrossRef]
50. Zargarian, S.S.; Rinoldi, C.; Ziai, Y.; Zakrzewska, A.; Fiorelli, R.; Gazińska, M.; Marinelli, M.; Majkowska, M.; Hottowy, P.; Mindur, B.; et al. Chronic Probing of Deep Brain Neuronal Activity Using Nanofibrous Smart Conducting Hydrogel-Based Brain–Machine Interface Probes. *Small Sci.* **2025**, *5*, 2400463. [CrossRef]
51. Qu, J.; Xie, K.; Chen, S.; He, X.; Wang, Y.; Chamberlin, M.; Zhao, X.; Zhu, G.; Xu, C.; Shi, P. Multifunctional hydrogel electronics for closed-loop antiepileptic treatment. *Sci. Adv.* **2024**, *10*, eadq9207. [CrossRef]
52. Shur, M.; Akouissi, O.; Rizzo, O.; Colin, D.J.; Kolinski, J.M.; Lacour, S.P. Revealing the complexity of ultra-soft hydrogel re-swelling inside the brain. *Biomaterials* **2023**, *294*, 122024. [CrossRef]
53. Hernandez-Ronquillo, L.; Thorpe, L.; Feng, C.; Hunter, G.; Dash, D.; Hussein, T.; Dolinsky, C.; Waterhouse, K.; Roy, P.L.; Jette, N. Diagnostic Accuracy of Ambulatory EEG vs Routine EEG in Patients With First Single Unprovoked Seizure. *Neurol. Clin. Pract.* **2023**, *13*, e200160. [CrossRef]

54. Jha, R.; Liu, D.D.; Gerstl, J.V.E.; Renauld, S.; Kilgallon, J.L.; Blitz, S.E.; Medeiros, L.; Nawabi, N.L.A.; Singh, H.; Chua, M.M.J.; et al. Comparative effectiveness of stereotactic, subdural, or hybrid intracranial EEG monitoring in epilepsy surgery. *J. Neurosurg.* **2024**, *141*, 372–380. [CrossRef]
55. Vansteensel, M.J.; Leinders, S.; Branco, M.P.; Crone, N.E.; Denison, T.; Freudenburg, Z.V.; Geukes, S.H.; Gosselaar, P.H.; Raemaekers, M.; Schippers, A.; et al. Longevity of a Brain–Computer Interface for Amyotrophic Lateral Sclerosis. *N. Engl. J. Med.* **2024**, *391*, 619–626. [CrossRef]
56. Greenspon, C.M.; Hobbs, T.G.; Verbaarschot, C.; Alamri, A.H.; Shelchkova, N.D.; Lienkämper, R.; Ye, J.; Simpson, T.W.; Weiss, J.M.; Weir, D.M.; et al. Long-term safety and efficacy of intracortical microstimulation in humans. *Sci. Transl. Med.* **2026**, *18*, eaec3728. [CrossRef]
57. Hsieh, J.C.; Alawieh, H.; Li, Y.; Iwane, F.; Zhao, L.; Anderson, R.; Abdullah, S.I.; Tang, K.W.K.; Wang, W.; Pyatnitskiy, I.; et al. A highly stable electrode with low electrode-skin impedance for wearable brain-computer interface. *Biosens. Bioelectron.* **2022**, *218*, 114756. [CrossRef]
58. Yao, Y.; Luo, J.; Hui, Y.; Lyu, J.; Ke, Y.; Shen, W.; Xu, Y.; Yu, Y.; Chen, H.; Chen, J.; et al. 3D-printed implantable bioelectronics enabled by anti-swelling and biphasic conductive hydrogels. *Nat. Mater.* **2026**. [CrossRef]
59. Roth, J.G.; Huang, M.S.; Navarro, R.S.; Akram, J.T.; LeSavage, B.L.; Heilshorn, S.C. Tunable hydrogel viscoelasticity modulates human neural maturation. *Sci. Adv.* **2023**, *9*, eadh8313. [CrossRef]
60. Won, D.; Kim, H.; Kim, J.; Kim, H.; Kim, M.W.; Ahn, J.; Min, K.; Lee, Y.; Hong, S.; Choi, J.; et al. Laser-induced wet stability and adhesion of pure conducting polymer hydrogels. *Nat. Electron.* **2024**, *7*, 475–486. [CrossRef]
61. Li, W.; Li, X.; Yang, M.; Liu, W.; Sun, R.; Peng, Y.; Wang, J.; Hu, Z.; Fang, K.; Liu, B.; et al. Robust Neural Interfaces Enabled by Non-Deformable Adhesive Hydrogel Patch for Stable Chronic ECoG Recording. *Adv. Funct. Mater.* **2025**, *35*, 2422717. [CrossRef]
62. Peng, J.; Li, X.; Li, W.; Gao, C.; Ma, C.; Zou, Z.; Yang, Y.; Liu, B.; Luo, Z.; Wang, X. Injectable Antifouling Adhesive Hydrogel Enables Robust Neural Interfaces for Stable ECoG Recording. *Adv. Healthc. Mater.* **2026**, *15*, e71397. [CrossRef]
63. Chen, L.; Zhong, H.; Wang, L.; Xu, L.; Fan, W.; Zhao, Y.; Zhang, H.; Shen, Y.; Wu, K.; Fu, X.; et al. Long-Term Stable Subdural Recordings Enabled by Fibrosis-Resistant Hydrogel-Integrated μECoG Arrays. *Adv. Sci.* **2025**, *12*, e15453. [CrossRef]
64. Yang, M.; Chen, P.; Qu, X.; Zhang, F.; Ning, S.; Ma, L.; Yang, K.; Su, Y.; Zang, J.; Jiang, W.; et al. Robust Neural Interfaces with Photopatternable, Bioadhesive, and Highly Conductive Hydrogels for Stable Chronic Neuromodulation. *ACS Nano* **2023**, *17*, 885–895. [CrossRef]
65. Yang, M.; Wang, L.; Liu, W.; Li, W.; Huang, Y.; Jin, Q.; Zhang, L.; Jiang, Y.; Luo, Z. Highly-stable, injectable, conductive hydrogel for chronic neuromodulation. *Nat. Commun.* **2024**, *15*, 7993. [CrossRef]
66. Huang, S.; Xiao, R.; Lin, S.; Wu, Z.; Lin, C.; Jang, G.; Hong, E.; Gupta, S.; Lu, F.; Chen, B.; et al. Anisotropic hydrogel microelectrodes for intraspinal neural recordings in vivo. *Nat. Commun.* **2025**, *16*, 1127. [CrossRef]
67. Xue, Y.; Chen, X.; Wang, F.; Lin, J.; Liu, J. Mechanically-Compliant Bioelectronic Interfaces through Fatigue-Resistant Conducting Polymer Hydrogel Coating. *Adv. Mater.* **2023**, *35*, 2304095. [CrossRef]
68. Oldroyd, P.; Gurke, J.; Malliaras, G.G. Stability of Thin Film Neuromodulation Electrodes under Accelerated Aging Conditions. *Adv. Funct. Mater.* **2023**, *33*, 2208881. [CrossRef]
69. Nguyen, C.K.; Geramifard, N.; Wu, Y.; Bhatt, M.; Joshi-Imre, A.; Negi, S.; Cogan, S.F. Electrical characterization and accelerated aging of amorphous silicon carbide implantable encapsulation. *J. Neural Eng.* **2025**, *22*, 066040. [CrossRef]
70. Shah Idil, A.; Lamont, C.; Nanbakhsh, K.; Mazza, F.; Giagka, V.; Constandinou, T.G.; Vanhoestenberghe, A.; Donaldson, N.D.N. On the stability of CMOS ICs with plasma-enhanced silicone encapsulation for active implantable neurotechnology: 4.3 years of accelerated life testing. *Front. Electron.* **2026**, *7*, 1788559. [CrossRef]
71. Killilea, J.; Lee, A.; Cuttaz, E.A.; Miceli, G.C.; Suquia, L.L.; Goding, J.A.; Chapman, C.A.R.; Green, R.A. "Spin-Rinse and Repeat": Facile Processing to Improve Cytocompatibility of Poly(3,4-Ethyelenedioxythiophene): Polystyrene Sulfonate Composites for Bioelectronics. *Adv. NanoBiomed Res.* **2025**, *5*, 2400149. [CrossRef]
72. Garg, R.; Laimo, F.A.; Ippolito, S.; Upadhyay, P.; Averbeck, S.R.; Boufidis, D.; Assenmacher, C.A.; Adewole, D.O.; Panigrahy, S.; Mohammadlou, B.S.; et al. Soft and Transient Bioelectronics Enabled by Polymer-Free $Ti_3C_2T_x$ MXene Hydrogels. *Adv. Mater.* **2026**, *38*, e75137. [CrossRef]
73. Wang, Y.; Han, M.; Jing, L.; Jia, Q.; Lv, S.; Xu, Z.; Liu, J.; Cai, X. Enhanced neural activity detection with microelectrode arrays modified by drug-loaded calcium alginate/chitosan hydrogel. *Biosens. Bioelectron.* **2025**, *267*, 116837. [CrossRef]
74. Lin, Z.K.; Lin, J.S.; Chen, Z.H.; Cheng, H.W.; Huang, W.C.; Chen, S.Y. Electrogelated drug-embedded silk/gelatin/rGO degradable electrode for anti-inflammatory applications in brain-implant systems. *J. Mater. Chem. B* **2024**, *12*, 1361–1371. [CrossRef]
75. Golabchi, A.; Wu, B.; Du, Z.J.; Cui, X.T. Long-Term Neural Recording Performance of PEDOT/CNT/Dexamethasone Coated Electrode Array Implanted in Visual Cortex of Rats. *Adv. NanoBiomed Res.* **2025**, *5*, 2400114. [CrossRef]
76. Li, L.; Hartzler, A.; Menendez-Lustri, D.M.; Zhang, J.; Chen, A.; Lam, D.V.; Traylor, B.; Quill, E.; Nethery, D.E.; Hoeferlin, G.F.; et al. Dexamethasone-loaded platelet-inspired nanoparticles improve intracortical microelectrode recording performance. *Nat. Commun.* **2025**, *16*, 8579. [CrossRef]

77. Turrin, G.; Crugeiras, J.; Bisquoli, C.; Barboni, D.; Catani, M.; Rodríguez-Meana, B.; Boaretto, R.; Albicini, M.; Caramori, S.; Trapella, C.; et al. Covalent Binding of Dexamethasone to Polyimide Improves Biocompatibility of Neural Implantable Devices. *Adv. Healthc. Mater.* **2025**, *14*, 2405004. [CrossRef]
78. Gori, M.; Giannitelli, S.M.; Vadalà, G.; Papalia, R.; Zollo, L.; Sanchez, M.; Trombetta, M.; Rainer, A.; Di Pino, G.; Denaro, V. A Soft Zwitterionic Hydrogel as Potential Coating on a Polyimide Surface to Reduce Foreign Body Reaction to Intraneural Electrodes. *Molecules* **2022**, *27*, 3126. [CrossRef]
79. Ren, L.; Hu, Y.; Ding, X.; Liao, M.; Shen, T.; Cao, S.; Zhang, H.; Cheng, H.; Qi, Y.; Feng, P.; et al. Multicargo Porous Cochlear Electrode Coating for Antifibrosis After Cochlear Implantation. *Adv. Sci.* **2025**, *12*, 2412158. [CrossRef]
80. Li, Y.; Wang, Z.; Pei, S.; Chen, R.; Li, Y.; Liang, Y.; Zhang, C.; Wang, L.; Dai, J.; Shi, L. Bisphosphonate-Based Hydrogel with pH-Responsive Minocycline Release Inhibits Microglia/Macrophages of M1 Polarization for Spinal Cord Injury Therapy. *ACS Mater. Lett.* **2024**, *6*, 553–565. [CrossRef]
81. Shen, H.; Xu, B.; Yang, C.; Xue, W.; You, Z.; Wu, X.; Ma, D.; Shao, D.; Leong, K.; Dai, J. A DAMP-scavenging, IL-10-releasing hydrogel promotes neural regeneration and motor function recovery after spinal cord injury. *Biomaterials* **2022**, *280*, 121279. [CrossRef]
82. Li, Y.; Liang, Y.; He, C.; Yao, R.; Jian, K.; Shi, L. A dual-drug sequential delivery hydrogel for programmatic microglia/macrophage polarization and function recovery in spinal cord injury. *Mater. Today Bio* **2025**, *35*, 102365. [CrossRef]
83. Gu, J.; Cai, X.; Raza, F.; Zafar, H.; Chu, B.; Yuan, H.; Wang, T.; Wang, J.; Feng, X. Preparation of a minocycline polymer micelle thermosensitive gel and its application in spinal cord injury. *Nanoscale Adv.* **2024**, *6*, 5874–5888. [CrossRef]
84. Li, Y.; Yang, C.; Fang, S.; Zhou, Y.; Li, M.; Liu, Z.; Zhang, X.; Duan, L.; Liu, K.; Sun, F. Clickable, Thermally Responsive Hydrogels Enabled by Recombinant Spider Silk Protein and Spy Chemistry for Sustained Neurotrophin Delivery. *Adv. Mater.* **2025**, *37*, 2413957. [CrossRef]
85. Meissner, S.; Rees, S.; Nguyen, L.; Connor, B.; Barker, D.; Harland, B.; Raos, B.; Svirskis, D. Encapsulation of the growth factor neurotrophin-3 in heparinised poloxamer hydrogel stabilises bioactivity and provides sustained release. *Biomater. Adv.* **2024**, *159*, 213837. [CrossRef]
86. Ramos Ferrer, P.; Vardhan, S.; Sakiyama-Elbert, S. Sustained neurotrophin-3 delivery from hyaluronic acid hydrogels for neural tissue regeneration. *J. Biomed. Mater. Res. Part A* **2024**, *112*, 1188–1199. [CrossRef]
87. Fan, C.; Yang, W.; Zhang, L.; Cai, H.; Zhuang, Y.; Chen, Y.; Zhao, Y.; Dai, J. Restoration of spinal cord biophysical microenvironment for enhancing tissue repair by injury-responsive smart hydrogel. *Biomaterials* **2022**, *288*, 121689. [CrossRef]
88. Sun, X.; Xiong, T.; Yang, K.; Wang, L.; Yang, W.; Zhao, H.; Gao, X.; You, Z.; Zhuang, Y.; Chen, Y.; et al. Individually Tailored Modular "Egg" Hydrogels Capable of Spatiotemporally Controlled Drug Release for Spinal Cord Injury Repair. *Adv. Healthc. Mater.* **2023**, *12*, 2301169. [CrossRef]
89. Su, W.; Xu, J.; Pei, D.; Li, X.; Yang, J.; Geng, Z.; Liu, Q.; Yang, L.; Yu, S. Hybrid Electrically Conductive Hydrogels with Local Nerve Growth Factor Release Facilitate Peripheral Nerve Regeneration. *ACS Appl. Bio Mater.* **2023**, *6*, 5854–5863. [CrossRef]
90. Liu, K.; Shao, J.; Han, B.; Liu, J.; Yan, S.; Liu, B.; Liu, Y. Conductive MeCbl/PEDOT:PSS/HA hydrogels with electrical stimulation for enhanced peripheral nerve regeneration. *Mater. Today Bio* **2025**, *32*, 101755. [CrossRef]
91. Liu, T.; Zhang, Q.; Li, H.; Cui, X.; Qi, Z.; Yang, X. An injectable, self-healing, electroconductive hydrogel loaded with neural stem cells and donepezil for enhancing local therapy effect of spinal cord injury. *J. Biol. Eng.* **2023**, *17*, 48. [CrossRef]
92. Zhang, R.; Zhang, M.; Chen, L.; Jiang, L.; Zou, C.; Li, N.; Zhou, H.; Feng, S. Dual-phase SilMA hydrogel: A dynamic scaffold for sequential drug release and enhanced spinal cord repair via neural differentiation and immunomodulation. *Front. Bioeng. Biotechnol.* **2024**, *12*, 1501488. [CrossRef]
93. Yu, Q.; Liu, S.; Guo, R.; Chen, K.; Li, Y.; Jiang, D.; Gong, S.; Yin, L.; Liu, K. Complete Restoration of Hearing Loss and Cochlear Synaptopathy via Minimally Invasive, Single-Dose, and Controllable Middle Ear Delivery of Brain-Derived Neurotrophic Factor–Poly(dl-lactic acid-co-glycolic acid)-Loaded Hydrogel. *ACS Nano* **2024**, *18*, 6298–6313. [CrossRef]
94. Wang, L.; Jiang, Y.; Yao, Y.; Deng, Y.; Liu, Z.; Ding, J.; Wang, W.; Chen, H.; Nan, K.; Li, L. Injectable drug-loaded thermosensitive hydrogel delivery system for protecting retina ganglion cells in traumatic optic neuropathy. *Regen. Biomater.* **2024**, *11*, rbae124. [CrossRef]
95. Meissner, S.; Lopez, S.; Rees, S.; O'Carroll, S.; Barker, D.; Harland, B.; Raos, B.; Svirskis, D. Safe subdural administration and retention of a neurotrophin-3-delivering hydrogel in a rat model of spinal cord injury. *Sci. Rep.* **2024**, *14*, 25424. [CrossRef]
96. Bansal, M.; Raos, B.; Aqrawe, Z.; Wu, Z.; Svirskis, D. An interpenetrating and patternable conducting polymer hydrogel for electrically stimulated release of glutamate. *Acta Biomater.* **2022**, *137*, 124–135. [CrossRef]
97. Aycan, D.; Karaca, F.; Koca, A.; Alemdar, N. Electro-stimulated drug release by methacrylated hyaluronic acid-based conductive hydrogel with enhanced mechanical properties. *Int. J. Biol. Macromol.* **2023**, *231*, 123297. [CrossRef]
98. Yoon, Y.; Shin, H.; Byun, D.; Woo, J.; Cho, Y.; Choi, N.; Cho, I.J. Neural probe system for behavioral neuropharmacology by bi-directional wireless drug delivery and electrophysiology in socially interacting mice. *Nat. Commun.* **2022**, *13*, 5521. [CrossRef]

99. Lin, Z.W.; Chen, Y.L.; Lei, W.L.; Ku, C.Y.; Su, P.Y.; Tai, L.C.; Tsai, T.H.; Liao, Y.T.; Chuang, A.E.Y.; Huang, W.C. Hierarchically structured conductive hydrogels for electrically programmable drug delivery in a diabetic wound healing electronic patch. *J. Control. Release* **2025**, *383*, 113760. [CrossRef]
100. Shi, Y.; Tang, Z.; Li, C.; Miao, Y.; Zhu, L.; Yue, B. Conductive Hydrogel Systems Enabling Rapid and Controllable Release of Guests at Low-Voltage Region. *Small* **2025**, *21*, 2410120. [CrossRef]
101. Abdel Aziz, I.; Gladisch, J.; Griggs, S.; Moser, M.; Biesmans, H.; Beloqui, A.; McCulloch, I.; Berggren, M.; Stavrinidou, E. Drug delivery via a 3D electro-swellable conjugated polymer hydrogel. *J. Mater. Chem. B* **2024**, *12*, 4029–4038. [CrossRef]
102. Cruz-Garza, J.G.; Bhenderu, L.S.; Taghlabi, K.M.; Frazee, K.P.; Guerrero, J.R.; Hogan, M.K.; Humes, F.; Rostomily, R.C.; Horner, P.J.; Faraji, A.H. Electrokinetic convection-enhanced delivery for infusion into the brain from a hydrogel reservoir. *Commun. Biol.* **2024**, *7*, 869. [CrossRef]
103. Mariello, M.; Ahnaf, F.; Proctor, C.M. Miniaturized, Flexible Electroosmotic Device Based on Laser-Patterned PEDOT:PSS Electrodes for Drug Delivery and Electrophysiological Biosensing. *Proc. Eurosens.* **2026**, *2026*, 198–199. [CrossRef]
104. Lee, H.; Song, S.; Ha, J.; Lee, Y.K.; Jang, K.I. A soft neural interface with a tapered peristaltic micropump for wireless drug delivery. *npj Flex. Electron.* **2025**, *9*, 85. [CrossRef]
105. Malekoshoaraie, M.H.; Wu, B.; Krahe, D.D.; Ahmed, Z.; Pupa, S.; Jain, V.; Cui, X.T.; Chamanzar, M. Fully flexible implantable neural probes for electrophysiology recording and controlled neurochemical modulation. *Microsyst. Nanoeng.* **2024**, *10*, 91. [CrossRef]
106. Hecko, S.; Vleugels, M.E.J.; Bayer, C.; Byun, D.; Hörberg, M.E.; Poremba, N.; Boukraa, R.; Keppel, P.; Löffler, A.; Kuba, W.; et al. Iontronic click-to-release enables electrically controlled delivery of drugs and biomolecules beyond charge and size limitations. *Nat. Commun.* **2026**, *17*, 4629. [CrossRef]
107. National Medical Products Administration. Announcement on Matters Concerning the Registration of Drug-Device Combination Products (No. 52 of 2021). 2021. Available online: https://yjj.sh.gov.cn/qtgzwj/20210728/9c39861d4e6e4acbb57c6c3e4e6db372.html (accessed on 7 October 2026).
108. National Medical Products Administration. Guidelines for Classification Determination of Brain-Computer Interface Medical Device Products. Announcement No. 24 of 2026. Available online: https://www.nmpa.gov.cn/directory/web/nmpa/xxgk/ggtg/ylqxggtg/ylqxqtggtg/20260630140449128.html (accessed on 10 November 2026).
109. Shanghai Medical Products Administration. Approval of the Implantable Brain-Computer Interface Hand Motor-Function Compensation System. Available online: https://yjj.sh.gov.cn/sjdt/20260313/274e66190b4a4fb8996b4d62334b1a6d.html (accessed on 26 October 2026).
110. National Medical Products Administration. Guidelines for Registration Review of Drug-Device Combination Products with a Medical Device as the Primary Mode of Action. Announcement No. 3 of 2022, Attachment 1. 2022. Available online: https://www.nmpa.gov.cn/ylqx/ylqxggtg/20220117145645132.html (accessed on 7 October 2026).
111. National Medical Products Administration. Guidelines for Registration Review of Qualitative and Quantitative Drug Characterization and In Vitro Release Studies for Drug-Device Combination Products with a Medical Device as the Primary Mode of Action. Announcement No. 3 of 2022, Attachment 2. 2022. Available online: https://www.nmpa.gov.cn/ylqx/ylqxggtg/20220117145645132.html (accessed on 7 October 2026).
112. State Administration for Market Regulation; Standardization Administration of China. GB/T 16886.1-2022 Biological Evaluation of Medical Devices-Part 1: Evaluation and Testing Within a Risk Management Process. 2022. Available online: https://openstd.samr.gov.cn/bzgk/std/newGbInfo?hcno=1650E4742A3734023A1E10CF0BCA0AE0 (accessed on 7 October 2026).
113. U.S. Food and Drug Administration. 21 CFR Part 3—Product Jurisdiction, Sections 3.2 and 3.4. Code of Federal Regulations. Available online: https://www.ecfr.gov/current/title-21/chapter-I/subchapter-A/part-3 (accessed on 7 October 2026).
114. U.S. Food and Drug Administration. Frequently Asked Questions About Combination Products. 2022. Available online: https://www.fda.gov/combination-products/about-combination-products/frequently-asked-questions-about-combination-products (accessed on 7 October 2026).
115. U.S. Food and Drug Administration. Implanted Brain-Computer Interface Devices for Patients with Paralysis or Amputation: Non-Clinical Testing and Clinical Considerations. Guidance for Industry and Food and Drug Administration Staff. 2021. Available online: https://www.fda.gov/regulatory-information/search-fda-guidance-documents/implanted-brain-computer-interface-bci-devices-patients-paralysis-or-amputation-non-clinical-testing (accessed on 7 October 2026).
116. U.S. Food and Drug Administration. Use of International Standard ISO 10993-1, Biological Evaluation of Medical Devices-Part 1: Evaluation and Testing within a Risk Management Process. Guidance for Industry and Food and Drug Administration Staff. 2023. Available online: https://www.fda.gov/regulatory-information/search-fda-guidance-documents/use-international-standard-iso-10993-1-biological-evaluation-medical-devices-part-1-evaluation-and (accessed on 7 October 2026).
117. U.S. Food and Drug Administration. Sprint Quattro Lead (6946M). PMA P920015, Supplement S306. Available online: https://www.accessdata.fda.gov/scripts/cdrh/cfdocs/cfpma/pma.cfm?ID=P920015S306 (accessed on 28 October 2026).

118. Prenzler, N.; Salcher, R.; Büchner, A.; Warnecke, A.; Kley, D.; Batsoulis, C.; Vormelcher, S.; Mitterberger-Vogt, M.; Morettini, S.; Schilp, S.; et al. Cochlear implantation with a dexamethasone-eluting electrode array: First-in-human safety and performance results. *Hear. Res.* **2025**, *461*, 109255. [CrossRef]
119. U.S. Food and Drug Administration. Quality Management System Regulation (QMSR). Available online: https://www.fda.gov/medical-devices/postmarket-requirements-devices/quality-management-system-regulation-qmsr (accessed on 2 February 2026).
120. U.S. Food and Drug Administration. Current Good Manufacturing Practice Requirements for Combination Products: Guidance for Industry and FDA Staff. 2017. Available online: https://www.fda.gov/media/90425/download (accessed on 26 October 2026).
121. European Parliament and Council. Regulation (EU) 2017/745 of 5 April 2017 on Medical Devices. Official Journal of the European Union, 2017, L117, 1-175. Article 1(8), Annex VIII Rule 14, and Annex IX Section 5.2. Available online: https://eur-lex.europa.eu/eli/reg/2017/745/oj (accessed on 7 October 2026).
122. Medical Device Coordination Group. MDCG 2022-5 Rev.1: Guidance on Borderline between Medical Devices and Medicinal Products under Regulation (EU) 2017/745 on Medical Devices. 2024. Available online: https://health.ec.europa.eu/document/download/b5a27717-229f-4d7a-97b1-e1c7d819e579_en?filename=mdcg_2022-5_en.pdf (accessed on 7 October 2026).
123. European Medicines Agency. Q&A for Applicants, Marketing Authorisation Holders of Medicinal Products and Notified Bodies Regarding Medicines Used in Combination with Medical Devices and Consultation Procedures for Certain Medical Devices. EMA/37991/2019 Rev.6. 2025. Available online: https://www.ema.europa.eu/en/documents/regulatory-procedural-guideline/questions-answers-implementation-medical-devices-vitro-diagnostic-medical-devices-regulations-eu-2017-745-eu-2017-746_en.pdf (accessed on 7 October 2026).
124. De Lauretis, A.; Eriksson Agger, A.; Pal, A.; Skov Pedersen, J.; Szostak, S.M.; Lund, R.; Lyngstadaas, S.P.; Ellingsen, J.E.; Linke, D.; Haugen, H.J. Balancing sterilization and functional properties in Poloxamer 407 hydrogels: Comparing heat and radiation techniques. *Regen. Biomater.* **2025**, *12*, rbaf005. [CrossRef]
125. Xie, X.; Rieth, L.; Williams, L.; Negi, S.; Bhandari, R.; Caldwell, R.; Sharma, R.; Tathireddy, P.; Solzbacher, F. Long-term reliability of Al_2O_3 and Parylene C bilayer encapsulated Utah electrode array based neural interfaces for chronic implantation. *J. Neural Eng.* **2014**, *11*, 026016. [CrossRef]
126. European Medicines Agency. Consultation procedure for ancillary medicinal substances in medical devices. Available online: https://www.ema.europa.eu/en/human-regulatory-overview/medical-devices/consultation-procedure-ancillary-medicinal-substances-medical-devices (accessed on 7 October 2026).

Disclaimer/Publisher's Note: The statements, opinions and data contained in all publications are solely those of the individual author(s) and contributor(s) and not of MDPI and/or the editor(s). MDPI and/or the editor(s) disclaim responsibility for any injury to people or property resulting from any ideas, methods, instructions or products referred to in the content.